UNIVERSIDADE ESTADUAL DE CAMPINAS
Faculdade de Engenharia Elétrica e de Computação

José Luis Hinostroza Ninahuanca

Contributions to communications systems using quaternion algebra

Contribuições aos sistemas de comunicações usando a álgebra de quatérnios

Campinas

2022

José Luis Hinostroza Ninahuanca

Contributions to communications systems using quaternion algebra

Contribuições aos sistemas de comunicações usando a álgebra de quatérnios

Thesis presented to the School of Electrical and Computer Engineering of the University of Campinas in partial fulfillment of the requirements for the degree of Doctor in Electrical Engineering, the area of Telecommunications and Telematics.

Tese apresentada à Faculdade de Engenharia Elétrica e de Computação da Universidade Estadual de Campinas como parte dos requisitos exigidos para a obtenção do título de Doutor em Engenharia Elétrica, na Àrea de Telecomunicações e Telemática

Supervisor: Prof. Dr. Luís Geraldo Pedroso Meloni

Este trabalho corresponde à versão final da tese defendida pelo aluno José Luis Hinostroza Ninahuanca, e orientada pelo Prof. Dr. Luís Geraldo Pedroso Meloni.

Campinas

2022

Ficha catalográfica
Universidade Estadual de Campinas
Biblioteca da Área de Engenharia e Arquitetura
Rose Meire da Silva - CRB 8/5974

H594c

Hinostroza Ninahuanca, José Luis, 1985-
Contributions to communications systems using quaternion algebra / José Luis Hinostroza Ninahuanca. – Campinas, SP : [s.n.], 2022.

Orientador: Luís Geraldo Pedroso Meloni.
Tese (doutorado) – Universidade Estadual de Campinas, Faculdade de Engenharia Elétrica e de Computação.

1. Quatérnios. 2. Telecomunicações - Codificação. 3. Multiplexação por divisão de frequência ortogonal. 4. Sincronização. I. Meloni, Luís Geraldo Pedroso, 1958-. II. Universidade Estadual de Campinas. Faculdade de Engenharia Elétrica e de Computação. III. Título.

Informações Complementares

Título em outro idioma: Contribuições aos sistemas de comunicações usando a álgebra de quatérnios
Palavras-chave em inglês:
Quatérnions
Space time codes
Orthogonal frequency division multiplexing
Synchronization
Área de concentração: Telecomunicações e Telemática
Titulação: Doutor em Engenharia Elétrica
Banca examinadora:
Luís Geraldo Pedroso Meloni [Orientador]
Renato da Rocha Lopes
Paulo Cardieri
Rui Seara
Pedro Henrique Juliano Nardelli
Data de defesa: 06-10-2022
Programa de Pós-Graduação: Engenharia Elétrica

Identificação e informações acadêmicas do(a) aluno(a)
- ORCID do autor: https://orcid.org/0000-0002-9756-7366
- Currículo Lattes do autor: http://lattes.cnpq.br/1248288571322829

COMISSÃO JULGADORA - TESE DE DOUTORADO

Candidato(a): José Luis Hinostroza Ninahuanca RA: 114941
Data de defensa: 06 de Outubro de 2022
Titulo da Tese: Contributions to communications systems using quaternion algebra

Prof. Dr. Luís Geraldo Pedroso Meloni (Presidente).
Prof. Dr. Renato da Rocha Lopes.
Prof. Dr. Paulo Cardieri.
Prof. Dr. Rui Seara.
Prof. Dr. Pedro Henrique Juliano Nardelli.

A Ata de Defesa, com as respectivas assinaturas dos membros da Comissão Julgadora, encontra-se no SIGA (Sistema de Fluxo de Dissertação/Tese) e na Secretaria de Pós-Graduação da Faculdade de Engenharia Elétrica e de Computação.

Dedico esta tesis a Ofelia, mi madre, a quien debo todo en la vida.

Acknowledgements

I would like to thank professor Luís Meloni, for his invaluable orientation, which went far beyond the academic realm. I never felt like just another student, but rather like part of his family. Moreover, I enjoyed working with him and with professor Osmar Tormena, whom I would also like to thank for his friendship and guidance during the research work. I hope that the end of this journey will be the beginning of a new academic partnership.

I also would like to thank my mother, Ofelia, for his unconditional love and continuous support. Likewise, I also thank my siblings Juan Carlos, Lucy and Jackeline for taking good care of her and for making the distance to seem smaller.

Last, but not least, I would like to thank my colleagues of Real-Time Digital Signal Processing Laboratory (RT-DSP): Jackelyn, Jaime, Gabriel T., Felipe, Roberto, Diego, Julio, Endrews, Silvio, Thales, Gabriel, Savio, and others. I truly appreciate every moment we shared at Unicamp, and I'm sure our friendship will continue for years to come.

This study was financed in part by the Coordenação de Aperfeiçoamento de Pessoal de Nível Superior – Brasil (CAPES) – Finance Code 001.

Finally, I'm grateful to the Serviço de Apoio ao Estudante (SAE), for making possible my permanence in Brazil during the first and last stages of the research.

“El gran error de la naturaleza humana es adaptarse. La verdadera felicidad está construida por un perpetuo estado de iniciación, de entusiasmo constante. (...) Ser el eterno forastero, el eterno aprendiz, el eterno postulante: he allí una forma para ser feliz”

Julio Ramón Ribeyro

Resumo

A busca contínua por melhorias de desempenho em sistemas de comunicações, expressadas como maiores taxas de transmissão, robustez contra o ruído, e eficiência espectral, entre outras, conduziu a academia para a exploração de novos esquemas e algoritmos de processamento de sinais nos extremos do transmissor e receptor. Entre eles, o uso da álgebra de quatérnios na representação e processamento dos sinais tem se mostrado como uma opção que permite não apenas simplicidade matemática, como também melhorias de desempenho em comparação à álgebra complexa tradicionalmente utilizada. Na presente tese, algoritmos clássicos de sincronismo em Multiplexão Ortogonal por Divisão de Frequência (OFDM) são reformulados usando quatérnios para ser aplicados em sinais OFDM de dupla polarização (DP), nas quais, as componentes horizontal e vertical são processadas como uma unidade, obtendo-se assim ganhos de desempenho demonstrados tanto de forma analítica como por simulações numéricas. Outra aplicação onde os quatérnios têm sido utilizados com sucesso é no projeto de códigos ortogonais e quase-ortogonais para sistemas de múltiplas entradas e múltiplas saídas (MIMO). Nessa área, a presente tese discute a aplicação flexível dos projetos ortogonais quaterniônicos (QOD) na exploração simultânea de diversidades de tempo, espaço e polarização em sistemas MIMO de dupla polarização.

Em resumo, o objetivo do presente trabalho é demostrar a aplicação da álgebra dos quatérnios nos sistemas de comunicação sem fio, ressaltando suas vantagens com relação aos esquemas clássicos baseados em álgebra complexa, com especial ênfase nos sistemas OFDM de dupla polarização tanto de entrada e saída única (SISO) como de múltiplas entradas e saídas (MIMO).

Palavras-chaves: Álgebra de quatérnios; códigos de bloco espaço-temporais; sincronismo em OFDM.

Abstract

The continuous search for enhanced performance of communications systems, in terms of increased data rate, higher noise immunity, and spectral efficiency, has led the academy to explore new schemes and algorithms for signal processing on both sides of the transmitter and receiver. Among them, the use of quaternion algebra for signal representation and processing turned up as an option that allows not only a mathematical simplification but also performance improvements when compared to the complex algebra traditionally used. In this thesis, we reformulate classical algorithms for OFDM synchronization, using quaternions, to be applied to dual-polarized (DP) OFDM signals by considering both polarization signals together as a single quaternion signal, thus obtaining performance gains that are proven by mathematical analysis as well as computer simulations. Another application, where quaternions have been successfully used, is in the design of orthogonal and semi-orthogonal codes for multiple-input multiple-output (MIMO) systems. In this area, the present thesis has shown the flexible application of quaternion orthogonal designs (QOD) to exploit simultaneously time, space, and polarization diversities in dual-polarized MIMO systems.

In summary, this research aims to demonstrate the application of quaternions algebra to wireless communications systems, highlighting its advantages compared to classical schemes based o complex algebra. Special attention was paid to dual-polarized OFDM, both single-input single-output (SISO) and MIMO.

Keywords: Quaternion algebra; space-time block codes; OFDM synchronization.

List of Figures

List of Tables

List of abbreviations and acronyms

CRLB	Cramer-Rao lower bound
DP	Dual-polarized.
HCA	Hypercomplex commutative algebra
i.i.d.	Independent and identically distributed
ISI	Inter-symbol interference
MIMO	Multiple-input multiple-output
ML	Maximum likelihood
OAM	Orthocomplex amplitude modulation
OFDM	Orthogonal frequency division multiplex
p.d.f.	Probability density function
QFT	Quaternion Fourier transform
QLMS	Quaternion least mean square
QOD	Quaternion orthogonal design
QOFDM	Quaternion OFDM
SIR	Signal to interference ratio
SNR	Signal to noise ratio
STO	Symbol time offset

List of symbols

$\boldsymbol{\mu}$	Pure unit quaternion.
Λ	Log-likelihood function
I_p	Identity matrix of order p
δ	Symbol time offset (STO)
ϵ	Carrier frequency offset (CFO)
N	FFT-length for OFDM/QOFDM
N_c	Cyclic prefix length
N_v	Number of virtual carriers
σ^2	Variance
M_t	Number of transmitter antennas
M_r	Number of receiver antennas
E_b	Energy of bit
N_0	Noise power spectral density

Contents

1 Introduction

Over the past decades, mobile communications have been characterized by their ever-increasing need for higher speed, reliability, and capacity as well as for reduced end-to-end latency and lower energy consumption, among others. One of the enabling technologies for 5G communications and beyond, intended to increase the capacity and reliability of communication links is massive Multiple-input multiple-output (MIMO) systems; they consist of the use of a high number of antennas both in the receiver and the transmitter sides; within these schemes, dual-polarized antennas provide additional diversity possibilities when used along with space and time diversity.

On the other hand, quaternion algebra, traditionally applied to approach 3-D navigation problems, has gained attention from the academy for its capacity to represent in a rich form signals from digital colored images, as well as communications signals using dual-polarized antennas. Therefore, it becomes important to study the application of quaternions to dual-polarized MIMO systems.

Besides, Orthogonal frequency division multiplex (OFDM) is a key technology adopted by a number of standards of wireless communications, due to its capacity of mitigating Inter-symbol interference (ISI) produced by the dispersive characteristics of wireless channels. Although the traditional application of OFDM to dual-polarized antennas performs the processing of both polarization signals in separate OFDM engines, the use of the Quaternion Fourier transform (QFT) allows the processing of those signals in a holistic form, which is called in literature as Quaternion OFDM (QOFDM) [1].

Nonetheless, despite all its benefits, OFDM is known to suffer from high sensitivity to time and frequency synchronization. A known result by Moose [2] establishes that a carrier frequency offset smaller than 4% of the carrier spacing is needed to guarantee a Signal to interference ratio (SIR) higher than 20dB. This drawback, which has been extensively studied by the academy, is inherited by QOFDM. Thus, the study of either new or adapted synchronization techniques for quaternion dual-polarized signals in QOFDM systems becomes relevant too.

Thereby, the research work presented in this thesis exploits the use of quaternion algebra in these two main problems, namely, MIMO dual-polarized systems and QOFDM synchronization. In that sense, this thesis show through mathematical development that classical algorithms intended to solve the related problems of these areas can be readily reformulated to be used in dual-polarized systems using quaternions. Besides, the benefits of this reformulated algorithm are shown analytically and by means of simulations.

1.1 Literature review

Quaternions were invented by Sir William Rowan Hamilton in 1843 [3] in what became one of the best-documented days in the history of mathematics. It was during a walk accompanied by his wife, along the Royal Canal in Dublin, when Hamilton got the vision of the fundamental equation

$$\boldsymbol{i}^2 = \boldsymbol{j}^2 = \boldsymbol{k}^2 = \boldsymbol{ijk} = -1, \tag{1.1}$$

relating the three hypercomplex roots of -1 that form a basis for quaternions. In honor of his discovery, a stone plaque has been placed in Broom Bridge, Ireland, near where it took place, which is shown in Figure 1.1.

Figure 1.1 – Hamilton's discovery of quaternions grabbed in a stone plaque on Broom Bridge - Dublin.

However, contrary to what can be thought, Hamilton's flash of insight was not just a moment of geniality, but the result of a period of more than ten years of trying to extend the properties of complex numbers to three-dimensional number systems. Soon after its discovery, Hamilton applied quaternions to space rotations in a way very similar to the one presented by Olinde Rodrigues [4], who expressed these rotations as matrix multiplications, with matrix elements dependent on a four-number set for all purposes equivalent to quaternions. For this fact, a controversy about quaternions discovery persists even until recent years [5]. Nevertheless, most authors consider Hamilton the discoverer because of his rigorous algebraic approach and Rodrigues' work on spatial rotation, the precursor to quaternion discovery.

A few decades after its introduction and despite Hamilton's expectations, quaternion algebra fell out of favor, being replaced by vectors [6] promoted by the mathematicians Gibbs and Heaviside. Later, however, but still in the 19th century, quaternions were the choice of Maxwell to synthesize its classical electromagnetism equations in 1873 [7] in disregard of Gibbs' vector system. Thereafter, in the past century, quaternion type-rotation groups found application in topics of theoretical physics, such as quantum mechanics [8], special relativity [9], and string theory, among others [10].

In the field of mathematics, quaternions form a non-commutative division ring, i.e., multiplication is non-commutative and a multiplicative inverse exists for every non-zero element of the set. Its discovery preceded, and also inspired, the notion of vectors, used by Gibbs and later by Heaviside to reformulate Maxwell's electromagnetic equations. Both quaternions and vectors converge into what is known actually as Clifford algebras.

In communications systems, the application of quaternions is more recent. In 1992, Ell [11] defined hypercomplex extensions of Fourier and Laplace transforms using quaternions as well as other hypercomplex commutative algebras (HCAs), he also applied them successfully to the analysis of two-dimensional linear time-invariant (LTI) systems. Later, Ell and Sangwine [12] used the quaternion Fourier transform (QFT) to analyze color images in the frequency domain, by considering the color components as parts of a quaternion number.

Later, Said et al. [13] used complex quaternions, denoted by Hamilton as 'biquaternions', to split the Fourier transform of a quaternion signal into four complex Fourier transforms. They also proved that the QFT applied over real quaternions exhibits symmetries similar to those present in the Fourier transform of real signals.

In 2006, Wysock et al. [14] proposed a simplified channel model for dual-polarized signals using a single quaternion variable, instead of the 2x2 complex matrix used in MIMO; they also used this model to simulate maximum likelihood (ML) detection over Rayleigh fading environments. Afterward, Seberry et al. [15] presented a detailed theory of quaternion orthogonal designs (QODs), intended to be used as orthogonal space-time-polarization block codes (STPBC) for dual-polarized MIMO systems.

The concept of analytic signal, first proposed by Gabor [16] and further studied by Ville [17], allows representing a real modulated signal by a complex signal with single side-band spectrum [18]. In [19], this concept was extended to include complex signals represented by quaternion hyperanalytic signals with single orthant spectrum. The hyperanalytic signal permits the characterization of a complex signal, probably composed of two independent real modulated signals, by its complex instantaneous amplitude (or envelope) and phase.

Analogously to how information can be carried in the instantaneous amplitude or phase in continuous wave modulation, a quaternion hyperanalytic signal allows carrying twice the amount of information in its complex envelope or phase. Nonetheless, the envelope recovery of the so-called Orthocomplex amplitude modulation (OAM) signal, exhibits an ambiguity problem that has been addressed by the author of this thesis in [20].

In 2012, Meloni [1] used quaternions and HCAs to model an OFDM system;

in that work, he showed through simulations that the choice of the hypercomplex axis for QFT has no impact on the overall performance of the system. Afterward, in [21], the authors extended the dual-polarized QOFDM scheme to MIMO systems, by implementing different combinations of space, time, and polarization diversities using the QODs proposed in the literature. More recently, in [22], Qureshi et al. demonstrated that every QOD obtained from iterative construction techniques allows linear decoupled decoding which reduces significantly the computational load in the receiver.

In adaptive signal processing, important for equalization in wireless communications characterized by time-varying channel fading, as well as in modern machine learning systems, quaternions have been successfully included. Quaternion least mean square (QLMS) has been introduced in [23], the calculation of quaternion gradient has considered both covariance and pseudocovariance in the same way as in the complex case. A further rigorous study of the derivatives of real-valued functions of quaternion vectors, named $\mathbb{HR}$ calculus after classic $\mathbb{CR}$ calculus, can be found in [24].

Other areas where quaternions have been successfully applied are vector-sensor signal processing [25], array processing [26], and adaptive filtering applied to dual-polarized channel equalization [27], among others.

1.2 Motivation and objectives

The continuous search for improved algorithms for wireless communications has motivated the exploration of this promising area. Even though this motivation led some researchers to produce the interesting results mentioned in the previous section, and to the best of author's knowledge, there were no studies on the application of quaternions to dual-polarized systems using OFDM, which is a widely adopted technique in fundamental technologies as mobile communications, WLAN, among others.

In that sense, a research group in the Real-Time Digital Signal Processing Laboratory (RT-DSP Lab) was formed to research on the use of quaternions in communication systems, by developing simulation tests aiming to assess its benefits. One of the early results of this work, previous to my group's incorporation, was the paper presented in the 2012 International Symposium on Communications and Information Technologies (ISCIT) [1] introducing QOFDM in the literature.

1.3 Main contributions

Throughout the research, two main topics were focused on, namely, quaternion coding for MIMO-OFDM and synchronization in dual-polarized QOFDM systems. The main contributions achieved in such topics are:

- To provide an overview of the technical literature about the applications of quaternions algebra to the communications field.
- Application of Quaternion orthogonal designs (QODs) to MIMO OFDM in order to exploit flexible combinations of space, time and polarization diversities simultaneously. In addition to providing an elegant approach, quaternions codes allow the use of Maximum likelihood (ML) decoding.
- Reformulation of OFDM synchronization methods using quaternion algebra and its application to dual-polarized quaternion OFDM. The proposed techniques exhibited improved performance when compared to their complex counterpart. Particularly, the variance of the Symbol time offset (STO) estimate for the proposed method exhibited a double slope in relation to the classical method. Thorough mathematical development, to find the theoretical limits of the proposed techniques, expressed as the well-known Cramer-Rao lower bound (CRLB), is presented and validated by means of simulations.

Besides, throughout the research work, the following papers were published or presented in symposium:

- Luís G.P. Meloni, José Luis Hinostroza Ninahuanca, Osmar Tormena Jr., "Construction and Analysis of Quaternion MIMO-OFDM Communications Systems", in Journal of Communication and Information Systems, vol. 32, No. 1, 2017. DOI: 10.14209/jcis.2017.9
- José Luis Hinostroza Ninahuanca, Osmar Tormena Jr., Silvio Oliveira S., Luís G.P. Meloni, "Improved CFO Synchronization of Dual-Polarized OFDM Systems using Training Symbols", presented in XXXVIII Simpósio Brasileiro de Telecomunicações e Processamento de Sinais - SBrT 2020.
- José Luis Hinostroza Ninahuanca, Osmar Tormena Jr., Luís G.P. Meloni, "Improved Time and Frequency Synchronization for Dual Polarization OFDM Systems", in Wiley ETRI Journal, vol. 43 No. 6, 2021. DOI: 10.4218/etrij.2021-0014

1.4 General outline

This thesis is structured in five chapters. Chapter 1 presents an introduction as well as a brief literature review concerning the application of quaternion algebra in communications systems and related areas. Chapter 2, composed of three sections, provides the theoretical background about quaternion algebra, dual-polarized quaternion OFDM, and Multiple-input multiple-output (MIMO) coding using quaternions, which serve as a basis for the subsequent development. Chapters 3 and 4 consist of the main contributions of the research. Each of these chapters is associated with the publications cited in the previous section.

Finally, Chapter 5 summarizes the main conclusions of the research and present a discussion about related future works.

2 Theoretical Reference

This chapter presents a general background about the topics treated throughout this research. Section 2.1 introduces some fundamental definitions and properties of quaternion algebra, with special attention to quaternion Fourier transform. In Section 2.2, the main characteristics of dual-polarized QOFDM are revisited. Section 2.3 presents a basic background about quaternion orthogonal designs intended to be used in MIMO systems. Finally, Section 2.4 briefly states the conclusions of the chapter.

2.1 Quaternion algebra

This section presents a brief review of quaternion algebra with special attention to quaternion Fourier transform, which is fundamental for later developments.

2.1.1 Definitions and main properties

Some fundamental definitions and properties used alongside the present thesis are presented.

Definition 2.1.1. The field of quaternions, denoted by $\mathbb{H}$ in honor of W. R. Hamilton, can be defined by the four-elements number $q \in \mathbb{H}$, composed of a real and three imaginary components, i.e.,

$$q = a + b\boldsymbol{i} + c\boldsymbol{j} + d\boldsymbol{k}, \tag{2.1}$$

where $a, b, c, d \in \mathbb{R}$ and $\{\boldsymbol{i}, \boldsymbol{j}, \boldsymbol{k}\}$ form a hypercomplex orthogonal basis numbers that obey the multiplication rules

$$\begin{gathered} \boldsymbol{i}^2 = \boldsymbol{j}^2 = \boldsymbol{k}^2 = \boldsymbol{ijk} = -1, \\ \boldsymbol{ij} = -\boldsymbol{ji} = \boldsymbol{k}, \quad \boldsymbol{jk} = -\boldsymbol{kj} = \boldsymbol{i}, \quad \boldsymbol{ki} = -\boldsymbol{ik} = \boldsymbol{j}, \end{gathered} \tag{2.2}$$

from which the non-commutative nature of multiplication in $\mathbb{H}$ results evident. However, it is still associative, i.e., given any three quaternions $q_1, q_2, q_3 \in \mathbb{H}$ we have $(q_1\, q_2)\, q_3 = q_1\,(q_2\, q_3)$.

The real components of q are denoted as $\Re\{q\} = a$, $\Im_i\{q\} = b$, $\Im_j\{q\} = c$ and $\Im_k\{q\} = d$.

Definition 2.1.2 (Scalar and pure quaternions)**.** A widely used decomposition splits a quaternion into its scalar and vector components, namely $q = S(q) + V(q)$, where $S(q) = a$, and $V(q) = b\boldsymbol{i} + c\boldsymbol{j} + d\boldsymbol{k}$ are the scalar and vector parts of q, respectively. Particularly, if $V(q) = 0$, q is named scalar quaternion, and if $S(q) = 0$, q is named vector or pure imaginary quaternion. $\mathbf{V}(\mathbb{H})$ denotes the set of pure imaginary quaternions.

Henceforth, q_s, $\vec{q}_v$ represent the scalar and vector parts of quaternion q, respectively. Furthermore, the arrow symbol $\vec{\{.\}}$ will be used to denote pure or vector quaternions.

A well-known property regarding the multiplication of pure quaternions follows.

Property 2.1.1 (Multiplication of pure imaginary quaternions)**.** *Given $\vec{p}, \vec{q} \in \mathbf{V}(\mathbb{H})$, it holds that*

$$\vec{p}\,\vec{q} = -\vec{p}\cdot\vec{q} + \vec{p}\times\vec{q}, \tag{2.3}$$

where $(\cdot)$ and $(\times)$ stand for the usual scalar and vector multiplication of three-dimensional vectors, respectively.

This property can be readily proved through the use of scalar and vector multiplication formulas. By using this property, a condition for commutativity in quaternion multiplication can be found.

Property 2.1.2 (Commutativity in quaternions multiplication)**.** *Let $p, q \neq 0, \in \mathcal{H}$, they are called commutable quaternion, i.e. $pq = qp$, if and only if, one of the following conditions are verified*

i) At least one of them is scalar, or

ii) $\exists \lambda \in \mathbb{R} \,/\, \vec{p}_v = \lambda \vec{q}_v$.

Proof. The first case, of multiplication by a scalar or between scalars, is straightforward. For the second part, considering the scalar-vector decompositions of p and q, it follows

$$pq = (p_s q_s + p_s\vec{q}_v + q_s\vec{p}_v + \vec{p}_v\vec{q}_v) \tag{2.4}$$

$$qp = (q_s p_s + q_s\vec{p}_v + p_s\vec{q}_v + \vec{q}_v\vec{p}_v). \tag{2.5}$$

From these equations, $pq = qp$ implies $\vec{p}_v\vec{q}_v = \vec{q}_v\vec{p}_v$. Then, using Property 2.1.1, the latter condition requires $\vec{p}_v \times \vec{q}_v = 0$, that is, $\vec{p}_v$ and $\vec{q}_v$ must be parallels in the sense of 3-D vectors. □

Definition 2.1.3 (Inner product and orthogonality)**.** The inner product of two quaternions $q_1 = a_1 + b_1\boldsymbol{i} + c_1\boldsymbol{j} + d_1\boldsymbol{k}$, $q_2 = a_2 + b_2\boldsymbol{i} + c_2\boldsymbol{j} + d_2\boldsymbol{k}$, denoted as $< q_1, q_2 >$ is their usual dot-product, i.e.

$$< q_1, q_2 >= a_1a_2 + b_1b_2 + c_1c_2 + d_1d_2. \tag{2.6}$$

If $< q_1, q_2 >= 0$, we say that q_1 and q_2 are orthogonal quaternions.

Obviously, any scalar is orthogonal to any pure imaginary quaternion. Besides, quaternions of the form $q_1 = a_1 + b_1\boldsymbol{i}$, and $q_2 = c_2\boldsymbol{j} + d_2\boldsymbol{k}$ are always orthogonal, and as each one of these degenerate quaternions has two degrees of freedom, they are said to lie in orthogonal planes. Furthermore, $\mathbb{H}$ can be generated by the direct sum of these orthogonal planes. The procedure of duplicating the order of an algebra using orthogonal elements is known as Cayley-Dickson construction, after the mathematicians Arthur Cayley and Leonard Dickson.

Definition 2.1.4 (Cayley-Dickson decomposition)**.** Cayley Dickson(CD) decomposition splits a quaternion into two complex numbers lying on orthogonal planes. Analogously to the way infinite pairs of orthogonal axes can generate the complex plane, there are infinite pairs of 'complex' orthogonal planes capable to produce the quaternion four-dimensional space. Among these, the one used throughout this thesis considers planes $\mathbb{C}_i$ and $\mathbb{C}_{jk}$, spanned by the basis $\{1, \boldsymbol{i}\}$ and $\{\boldsymbol{j}, \boldsymbol{k}\}$, respectively, i.e.,

$$q = z_1 + z_2\boldsymbol{j}, \tag{2.7}$$

where $z_1 = a + b\boldsymbol{i}$ is called simplex part of q, and denoted $\mathcal{S}(q)$, and $z_2 = c + d\boldsymbol{i}$ is called perplex part of q, and denoted $\mathcal{P}(q)$. An important insight is obtained from (2.7), where right-side multiplication of plane $\mathbb{C}_i$ by $\boldsymbol{j}$ generates the orthogonal plane $\mathbb{C}_{jk}$, and both together span $\mathbb{H}$, in the same way as the real and imaginary axes of 2-D Argand plane span $\mathbb{C}$.

Definition 2.1.5 (Conjugation)**.** The conjugate of a quaternion is obtained by opposing the three imaginary parts, namely $q^* = a - b\boldsymbol{i} - c\boldsymbol{j} - d\boldsymbol{k} = S(q) - V(q)$, or, in terms of its CD components, $q^* = z_1^* - z_2\boldsymbol{j}$, where complex conjugation was used in right side.

Different from its complex counterpart, quaternion conjugation is not an involution, but an anti-involution operation, i.e., it distributes over a product by reversing the order of factors, that is $(q_1q_2)^* = q_2^*q_1^*$, this property readily extends to any number of factors.

An interesting lemma, derived in [28], allows us to reduce the computational complexity of left-right side quaternion multiplication of a complex number when we are interested only in the real part of the result.

Lemma 1. For $a, b \in \mathbb{H}$ and $z \in \mathbb{C}_i$, the following relation is valid

$$\mathcal{R}\{azb\} = \mathcal{R}\{\mathcal{S}\{a^*b^*\}z^*\}. \tag{2.8}$$

Proof. With this aim, consider the expressions of the simplex and perplex components of a quaternion product as a function of the components of each factor, let the CD decomposition $a = \mathcal{S}\{a\} + \mathcal{P}\{a\}\boldsymbol{j}$, $b = \mathcal{S}\{b\} + \mathcal{P}\{b\}\boldsymbol{j}$, where $\mathcal{S}\{a\}, \mathcal{P}\{a\} \in \mathbb{C}_i$ are the simplex and perplex parts of a, and $\mathcal{S}\{b\}, \mathcal{P}\{b\}$ are those corresponding to b, respectively.

Also, let $ab = \mathcal{S}\{ab\} + \mathcal{P}\{ab\}\boldsymbol{j}$ and $a^*b^* = \mathcal{S}\{a^*b^*\} + \mathcal{P}\{a^*b^*\}$, it is easy to verify that

$$\mathcal{S}\{ab\} = \mathcal{S}\{a\}\mathcal{S}\{b\} - \mathcal{P}\{a\}\mathcal{P}\{b\}^*, \tag{2.9}$$

$$\mathcal{P}\{ab\} = \mathcal{S}\{a\}\mathcal{P}\{b\} + \mathcal{P}\{a\}\mathcal{S}\{b\}^*, \tag{2.10}$$

$$\mathcal{S}\{a^*b^*\} = \mathcal{S}\{a\}^*\mathcal{S}\{b\}^* - \mathcal{P}\{a\}\mathcal{P}\{b\}^*, \tag{2.11}$$

$$\mathcal{P}\{a^*b^*\} = -\mathcal{S}\{a\}^*\mathcal{P}\{b\} + \mathcal{P}\{a\}\mathcal{S}\{b\}. \tag{2.12}$$

Besides, it is evident that taking the real part of a quaternion is equivalent to taking the real part just from its simplex part. Therefore, $\mathcal{R}\{azb\} = \mathcal{R}\{\mathcal{S}\{azb\}\}$, now using (2.9), considering zb as the second quaternion in the product

$$\mathcal{R}\{azb\} = \mathcal{R}\{\mathcal{S}\{a\}\mathcal{S}\{zb\} - \mathcal{P}\{a\}\mathcal{P}\{zb\}^*\} \tag{2.13}$$

$$= \mathcal{R}\{\mathcal{S}\{a\}z\mathcal{S}\{b\} - \mathcal{P}\{a\}z^*\mathcal{P}\{b\}^*\} \tag{2.14}$$

$$= \mathcal{R}\{\mathcal{S}\{a\}^*z^*\mathcal{S}\{b\}^* - \mathcal{P}\{a\}z^*\mathcal{P}\{b\}^*\} \tag{2.15}$$

$$= \mathcal{R}\{[\mathcal{S}\{a\}^*\mathcal{S}\{b\}^* - \mathcal{P}\{a\}\mathcal{P}\{b\}^*]z^*\}, \tag{2.16}$$

where the third equality comes from $\mathcal{R}\{z\} = \mathcal{R}\{z^*\}$. Finally, from (2.11), it comes the lemma identity

$$\mathcal{R}\{azb\} = \mathcal{R}\{\mathcal{S}\{a^*b^*\}z^*\}. \tag{2.17}$$

□

Notice that, while the left side of (2.8) implies one complex quaternion and one quaternion multiplication, the right side requires only one quaternion multiplication and one complex multiplication. Thus, there is a computational gain that justifies the use of (2.8).

Definition 2.1.6 (Norm and module)**.** Analogously to complex numbers, the norm of q is defined by $\|q\| = qq^* = q^*q = a^2 + b^2 + c^2 + d^2$, and its module $|q| = \sqrt{\|q\|}$. Also, as in complex case, both operations are distributive over multiplication, i.e. $\|q_1\, q_2\| = \|q_1\|\|q_2\|$.

If $|q| = 1$, q is called unit quaternion. It is easy to prove that the solutions of $q^2 = -1$ are the set of pure unit quaternion, which are denoted by using bold type throughout this thesis. In other words, the hypercomplex roots of -1 are the set of points in the surface of the unitary sphere centered at the origin of the 3D space of axes $\boldsymbol{i}, \boldsymbol{j}$, and $\boldsymbol{k}$.

Throughout this thesis, we adopt as a convention that $\boldsymbol{\mu}$ stands for any pure unit quaternion, that is, $\boldsymbol{\mu} \in \mathbf{V}(\mathbb{H})$ and $|\boldsymbol{\mu}| = 1$. Also, $\boldsymbol{\mu}^\perp$ stands for a pure unit quaternion orthogonal to $\boldsymbol{\mu}$. Finally, $\tilde{q}$ denotes the versor associated to q, that is, $\tilde{q} = \dfrac{q}{|q|}$.

Definition 2.1.7 (Equivalence and involutions)**.** Two quaternions q_1 and q_2 are called similar or equivalent, denoted by $q_1 \sim q_2 \iff \exists \nu \in \mathbb{H}$, $\nu \neq 0$, such that [24]

$$q_1 = \nu q_2 \nu^{-1}. \tag{2.18}$$

From (2.18), it is straightforward that $S(q_1) = S(q_2)$ and $\|q_1\| = \|q_2\|$. Furthermore, it implies that $V(q_1)$ can be obtained from $V(q_2)$ through a rotation around an axis parallel to ν. From this definition, it follows that $\boldsymbol{i} \sim \boldsymbol{j} \sim \boldsymbol{k}$, and also $q \sim q^*$.

In the particular case where ν is a pure unit quaternion, the right side of (2.18) represents an involution operation, i.e., an operation that when applied twice produces the original value. Using $\boldsymbol{\mu}$ as usual for pure unit quaternion,

$$\overline{q}^{\boldsymbol{\mu}} = -\boldsymbol{\mu}\, q\, \boldsymbol{\mu} \tag{2.19}$$

denotes the general involution operation with respect to the $\boldsymbol{\mu}$ axis. It can be verified that $\overline{q_1 q_2}^{\boldsymbol{\mu}} = \overline{q_2}^{\boldsymbol{\mu}} \overline{q_1}^{\boldsymbol{\mu}}$, thus $\overline{\{.\}}^{\mu}$ is, sometimes, referred as quaternion anti-involution.

If $\boldsymbol{\mu}$ is chosen among the standard basis elements of $\mathbb{H}$, i.e.,$\{\boldsymbol{i}, \boldsymbol{j}, \boldsymbol{k}\}$, three canonical involutions are obtained,

$$\begin{aligned}
\overline{q}^{\boldsymbol{i}} &= -\boldsymbol{i}\, q\, \boldsymbol{i} = a + b\boldsymbol{i} - c\boldsymbol{j} - d\boldsymbol{k} \\
\overline{q}^{\boldsymbol{j}} &= -\boldsymbol{j}\, q\, \boldsymbol{j} = a - b\boldsymbol{i} + c\boldsymbol{j} - d\boldsymbol{k} \\
\overline{q}^{\boldsymbol{k}} &= -\boldsymbol{k}\, q\, \boldsymbol{k} = a - b\boldsymbol{i} - c\boldsymbol{j} + d\boldsymbol{k}.
\end{aligned} \tag{2.20}$$

Clearly, the four real components of a quaternion can be recovered through linear combinations of itself and its involutions, i.e.,

$$\Re\{q\} = \frac{1}{4}(q + \overline{q}^{\boldsymbol{i}} + \overline{q}^{\boldsymbol{j}} + \overline{q}^{\boldsymbol{k}}) \tag{2.21}$$

$$\Im_i\{q\} = \frac{1}{4\boldsymbol{i}}(q + \overline{q}^{\boldsymbol{i}} - \overline{q}^{\boldsymbol{j}} - \overline{q}^{\boldsymbol{k}}) \tag{2.22}$$

$$\Im_j\{q\} = \frac{1}{4\boldsymbol{j}}(q - \overline{q}^{\boldsymbol{i}} + \overline{q}^{\boldsymbol{j}} - \overline{q}^{\boldsymbol{k}}) \tag{2.23}$$

$$\Im_k\{q\} = \frac{1}{4\boldsymbol{k}}(q - \overline{q}^{\boldsymbol{i}} - \overline{q}^{\boldsymbol{j}} + \overline{q}^{\boldsymbol{k}}) \tag{2.24}$$

Definition 2.1.8 (Exponential of quaternion)**.** The exponential of a quaternion is defined through its Maclaurin series expansion, i.e.

$$e^q = 1 + \frac{q^1}{1!} + \frac{q^2}{2!} + \frac{q^3}{3!} + \ldots = \sum_{n=0}^{+\infty} \frac{q^n}{n!}. \tag{2.25}$$

Property 2.1.3. *The known property of the exponential of real and complex numbers*

$$e^{q_1 + q_2} = e^{q_1} e^{q_2} = e^{q_2} e^{q_1} \tag{2.26}$$

verifies in $\mathbb{H}$ *only* $\iff$ q_1 *and* q_2 *are commutable quaternions.*

As a consequence of properties 2.1.3 and 2.1.2, for any quaternion $q = q_r + \vec{q}_v$, $e^q = e^{q_r} e^{\vec{q}_v}$.

Definition 2.1.9 (Euler formula). Let $\vec{q} \in \mathbb{V}(\mathbb{H})$, be a pure quaternion. From definition 2.1.8 and by use of property 2.1.1, it can be shown that

$$e^{\vec{q}} = \cos(|\vec{q}|) + \frac{\vec{q}}{|\vec{q}|}\sin(|\vec{q}|), \tag{2.27}$$

or, given $\rho_{\vec{q}} = |\vec{q}|$, and $\boldsymbol{\mu}_{\vec{q}} = \dfrac{\vec{q}}{|\vec{q}|}$,

$$e^{\vec{q}} = e^{\rho_{\vec{q}}\boldsymbol{\mu}_{\vec{q}}} = \cos(\rho_{\vec{q}}) + \boldsymbol{\mu}_{\vec{q}}\sin(\rho_{\vec{q}}), \tag{2.28}$$

which is the quaternion form of Euler's formula.

In (2.28), it should be noted that the exponential of a vector quaternion exhibits a periodicity of fundamental period $2\pi\boldsymbol{\mu}_q$, similar to the $2\pi\boldsymbol{i}$ periodicity of the complex exponential e^z. Furthermore, it is readily observable that the right side of (2.28) represents a unit quaternion with their three corresponding degrees of freedom; that is to say, any unit quaternion can be expressed as the exponential of a pure quaternion taken from a set of collinear vector quaternions. In fact, as the pair $(2\pi - \rho_{\vec{q}}, -\boldsymbol{\mu}_{\vec{q}})$ produces, on the right side of (2.28), the same unit quaternion than the pair $(\rho_{\vec{q}}, \boldsymbol{\mu}_{\vec{q}})$, there exist two sets of collinear vector quaternions able to represent the same unit quaternion.

For non-pure quaternions $q = q_r + \vec{q}_v$, from definition 2.1.9 and property 2.1.3, it is straightforward that

$$e^q = e^{q_r}[cos(|\vec{q}_v|) + \boldsymbol{\mu}_{\vec{q}_v}\sin(|\vec{q}_v|)], \tag{2.29}$$

where $\boldsymbol{\mu}_{\vec{q}_v} = \dfrac{\vec{q}_v}{|\vec{q}_v|}$.

Definition 2.1.10 (Logarithm). Given $q = q_r + \vec{q}_v$, the logarithm of q is defined as

$$\ln(q) = \ln(|q|) + \frac{\vec{q}_v}{|\vec{q}_v|}\arccos(\frac{q_r}{|q|}), \tag{2.30}$$

where the use of the arccos function prevents the logarithm from being multivalued, which could result from the previous discussion about unit quaternion expressed as the exponential of pure quaternions.

Definition 2.1.11 (Inverse and division). The fact that quaternions are a normed algebra implies the existence of a multiplicative inverse for every nonzero element, namely, $q^{-1} = \dfrac{q^*}{\|q\|}$, for $q \neq 0$. Then, quaternion division is defined as $\dfrac{q_1}{q_2} = q_1\, q_2^{-1}$, where, again, the order of multiplication is important.

By use of Euler's formula, a quaternion can also be decomposed in polar form, analogously to the complex case.

Definition 2.1.12 (Polar form of quaternions)**.** From (2.28), the exponential of a pure quaternion results in a unit quaternion; equivalently, any unit quaternion can be expressed as the exponential of a pure or vector quaternion. Following this reasoning, it can be shown that any quaternion $q = q_r + \vec{q}_v$ can be written in the form

$$q = \rho e^{\boldsymbol{\mu}\theta} \quad \text{with} \begin{cases} \rho & = |q| \\ \boldsymbol{\mu} & = \dfrac{\vec{q}}{|\vec{q}|} \\ \theta & = \arctan\left(\dfrac{|\vec{q}|}{q_r}\right) \end{cases} \tag{2.31}$$

Two remarks must be made regarding (2.31). First, it establishes that any quaternion can be represented by the set $(\rho, \boldsymbol{\mu}, \theta)$ formed by two real numbers and a pure unit quaternion. As already mentioned, $\boldsymbol{\mu}$ can be seen as a point on the surface of the three-dimensional unit sphere, thus it can be characterized by two angles such as azimuth and elevation. Therefore, it turns out that the original quaternion can be expressed, again, by four real quantities, in this case, a positive real number and three angles.

The second remark in (2.31) is that because of the π period of the tangent function, the angle θ belongs to the interval $[0, \pi]$, in contrast to the complex case where it can be any angle in $[0, 2\pi]$. A direct consequence of this is that the triplet $(\rho, -\boldsymbol{\mu}, 2\pi - \theta)$ also produces the same quaternion when substituted into (2.31).

Definition 2.1.13 (Polar Cayley Dickson form)**.** It is possible to obtain a polar representation of a not-null quaternion based on Cayley-Dickson decomposition [29]. Given $q = z_1 + z_2\boldsymbol{j}$, it can be expressed as

$$q = Ae^{B\boldsymbol{j}}, \tag{2.32}$$

where $A \in \mathbb{C}_i$ is the complex modulus, and $B \in \mathbb{C}_i$ is the complex phase of q.

$$A = \frac{z_1}{|z_1|}|q| \tag{2.33}$$

$$B = -(\ln[A^{-1}q])\boldsymbol{j}. \tag{2.34}$$

There is a sign ambiguity in the calculation of A, from (2.32). Thus, (2.33) represents the positive solution. A detailed derivation of the complex amplitude and phase as well as a discussion about this ambiguity can be found in [29].

A more comprehensive treatment of quaternion algebra is beyond the scope of this thesis; interested readers are referred to [3, 30, 31].

2.1.2 Hypercomplex commutative algebras

The non-commutativity of quaternion multiplication led researchers to devise the so-called Hypercomplex commutative algebras (HCAs) that overcome this problem at the cost of not being division algebras, i.e., they lack a multiplicative inverse. These HCA differ in the choice of the hypercomplex root of 1, they are

- HCA-i: First introduced by Ell [11], it uses $\boldsymbol{i}^2 = 1$. ($\boldsymbol{i} \notin \mathbb{R}$).
- HCA-j: Presented by Pei [32], it uses $\boldsymbol{j}^2 = 1$.
- HCA-k: Proposed by Delsuc [33], it uses $\boldsymbol{k}^2 = 1$.

An interesting approach to the HCA-k, from the perspective of signal processing, is found in [34], where the authors refer to this system as commutative (2,2)-model of quaternions.

2.1.3 Quaternion discrete Fourier transform (QDFT)

Early extensions of Fourier transform (FT) to hypercomplex numbers are found in [33], [11], and [32]. These works introduced the hypercomplex Fourier transform (hFT) of a bivariate function of time $f(t, \tau)$. This hFT is a bivariate function of two independent frequency variables $F(\omega, \nu)$ valued in any of the HCAs described in 2.1.2. These algebras solve the non-commutativity issue of quaternion multiplications, with the limitation of not being division rings, i.e., the existence of a unique multiplicative inverse for any not null element is not granted for these HCAs.

The left-sided quaternion Fourier transform (QFT) of a quaternion-valued function $f : \mathbb{R} \to \mathbb{H}$ w.r.t. the hypercomplex axis $\boldsymbol{\mu}$, defined in [35], as

$$F_\mu(\omega) = \int_{-\infty}^{\infty} e^{-\boldsymbol{\mu}\omega t} f(t) dt, \tag{2.35}$$

where, as already mentioned, $\boldsymbol{\mu}$ stands for any pure unit quaternion. Throughout this thesis, we use $\boldsymbol{\mu} = \boldsymbol{i}$ as the hypercomplex axis for QFT calculation, i.e.,

$$F(\omega) = \int_{-\infty}^{\infty} e^{-\boldsymbol{i}\omega t} f(t) dt. \tag{2.36}$$

If we consider the CD decomposition $f(t) = z_1(t) + z_2(t)\boldsymbol{j}$, where $z_1(t), z_2(t) \in \mathbb{C}_{\boldsymbol{i}}$, the simplex and perplex parts of $F(\omega)$ can be obtained through the calculation of complex FT of $z_1(t)$ and $z_2(t)$, respectively. Therefore, most of the properties of classical FT remain valid for QFT, since we use the same hypercomplex axis, and we respect the order of multiplications. Evidently, if the perplex part of $f(t)$ vanishes, i.e., $z_2(t) = 0$, then (2.36) reduces to the classical FT formula.

Since the focus of this work is on digital communications, we use the discrete version of (2.36). Thus, the pair of QDFT $f[n] \rightleftharpoons F[u]$ is calculated as

$$F[u] = \sum_{n=0}^{N-1} \exp\left(-\boldsymbol{i}2\pi\frac{nu}{N}\right) f[n], \tag{2.37}$$

$$f[n] = \frac{1}{N}\sum_{u=0}^{N-1} \exp\left(\boldsymbol{i}2\pi\frac{nu}{N}\right) F[u], \tag{2.38}$$

for $n, u = 0, 1, ..., N-1$.

2.1.4 Quaternion multivariate Gaussian distribution

Let $\boldsymbol{X} = [X_1\, X_2\, ...\, X_p]^T$, a $p \times 1$ vector of quaternion random variables (r.v.'s), $\boldsymbol{X}$ is said to have Gaussian or normal distribution if its joint p.d.f. is given by [36]

$$f_{\boldsymbol{X}}(\boldsymbol{x}) = \left(\frac{\pi}{2}\right)^{-2p} |\mathbf{K}_{\boldsymbol{X}}|^{-2} \exp\{-2(\boldsymbol{x} - \boldsymbol{m}_{\boldsymbol{X}})^H \mathbf{K}_{\boldsymbol{X}}^{-1} (\boldsymbol{x} - \boldsymbol{m}_{\boldsymbol{X}})\}, \tag{2.39}$$

where $\boldsymbol{m}_{\boldsymbol{X}} = \mathrm{E}[\boldsymbol{X}]$ and $\mathbf{K}_{\boldsymbol{X}} = \mathrm{E}[(\boldsymbol{X} - \boldsymbol{m}_{\boldsymbol{X}})(\boldsymbol{X} - \boldsymbol{m}_{\boldsymbol{X}})^H]$ are the expected value and covariance matrix of $\boldsymbol{X}$, respectively. Analogously to real and complex random vectors, the notation $\boldsymbol{X} \sim \mathrm{QN}(\boldsymbol{m}_{\boldsymbol{X}}, \mathbf{K}_{\boldsymbol{X}})$ is used.

For a single quaternion random variable $X \sim \mathrm{QN}(m_x, \sigma^2)$, the p.d.f. is obtained by setting $p = 1$ in (2.39), i.e.,

$$f_X(x) = \frac{4}{\pi^2\sigma^4} \exp\left\{\frac{-2|x - m_x|^2}{\sigma^2}\right\} \tag{2.40}$$

For a vector $\boldsymbol{X}$ of zero-mean and *i.i.d.* quaternion random variables, i.e., $\mathrm{E}[X_i] = 0$ and $\mathrm{E}[X_i X_j^*]) = \sigma_x^2 \delta_{ij}$, obviously $\mathbf{K}_{\boldsymbol{X}} = \sigma_x^2 \mathrm{I_p}$. Therefore, from (2.39)

$$f_{\boldsymbol{X}}(\boldsymbol{x}) = \left(\frac{2}{\pi\sigma_x^2}\right)^{2p} \exp\left\{\frac{-2|\boldsymbol{x}|^2}{\sigma_x^2}\right\} \tag{2.41}$$

It must be clarified that (2.40) is valid only when $\boldsymbol{X}$ is a proper quaternion random vector. The concept of properness, originally proposed for complex random processes [37] implies a vanishing pseudo-covariance. Furthermore, circular symmetry for complex random variables is equivalent to properness. For quaternions, the extension of this concept is not trivial [36]. Nonetheless, for the scenarios studied alongside the present thesis, unless otherwise stated, we model additive white Gaussian noise (AWGN), in dual-polarized channels, as being formed by four i.i.d. real random processes, thus, properness is granted and the p.d.f. formula of (2.41) for quaternion vector random variables can be applied to any subset of the process.

2.1.5 Quaternion algorithms for adaptive systems

Many algorithms for adaptive systems have been recently extended to quaternions algebra. In this section, the most important ones which can be used for synchronization and channel equalization are mentioned. Figure 2.1 shows a block diagram of the adaptive filter problem considered in this section, where $d(n)$ stands for the desired or reference signal, whereas $x(n)$ is an input signal that we intend to process through a filter in order to obtain the closest approximation to $d(n)$, or, equivalently, to minimize the error signal $e(n)$.

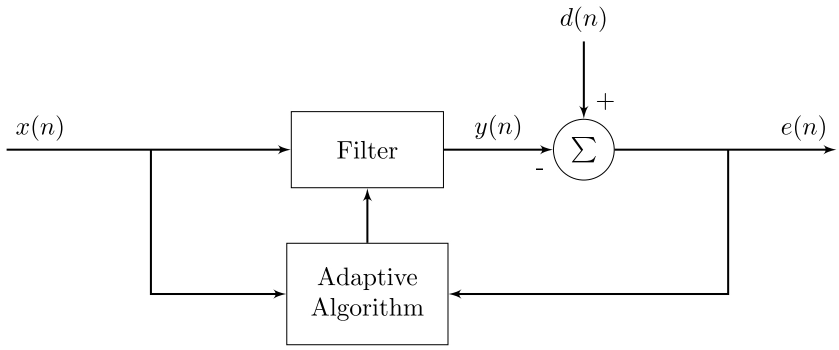

Figure 2.1 – Block diagram of a typical adaptive filtering setup.

2.1.5.1 Quaternion LMS

Quaternion least-mean-square (QLMS) is derived using the method of stochastic gradient [23], [24], [38]. The cost function is calculated analogously to real and complex cases, i.e., $\mathcal{J}(n) = e(n)e^*(n)$, where the error vector is $e(n) = d(n) - \mathbf{w}^T(n)\mathbf{x}(n)$.

Minimization of the stochastic gradient of $\mathcal{J}(n)$, taking into consideration the non-commutative nature of quaternions [24], leads to the coefficient update formula, i.e.,

$$\mathbf{w}(n+1) = \mathbf{w}(n) + \mu(2e(n)x^*(n) - x^*(n)e(n)). \tag{2.42}$$

2.1.5.2 Quaternion widely linear least-mean-square (WL-LMS)

The widely linear model allowed significant improvements in estimation problems with complex input data [39] for which the circular condition is not fulfilled. This extended model considers not only the complex input signal but also its complex conjugate, as shown in Figure (2.2). The output of the widely linear estimator is

$$\boldsymbol{y} = \boldsymbol{h}^T\boldsymbol{x} + \boldsymbol{g}^T\boldsymbol{x}^*, \tag{2.43}$$

where both $\boldsymbol{h}$ and $\boldsymbol{g}$ are the filter coefficients found through optimization of the real cost function. Equation (2.43) can be expressed as $y = [\boldsymbol{w}^a]^T\boldsymbol{x}^a$, where $\boldsymbol{w}^a = [\boldsymbol{h}^T\, \boldsymbol{g}^T]^T$, and $\boldsymbol{x}^a = [\boldsymbol{x}^T\, \boldsymbol{x}^H]^T$, are called augmented variables. The impossibility of getting derivatives

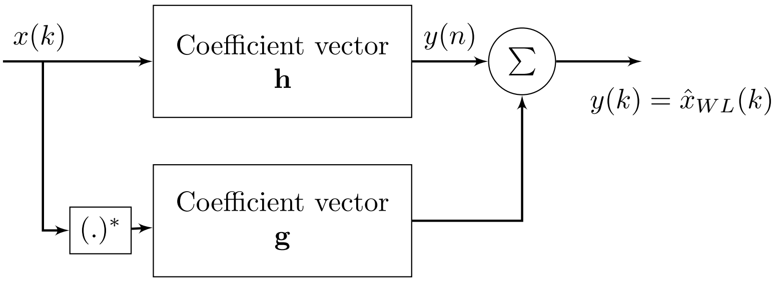

Figure 2.2 – Widely linear filtering model.

of real functions of complex variables in classic complex analysis led to the definition of complex gradient [40], and the further development of the so-called $\mathbb{CR}$ calculus [41].

The extension of these developments to quaternions, named $\mathbb{HR}$ calculus, was proposed by Mandic [24] et al. In that work, a quaternion-valued function $f : \mathbb{H} \rightarrow \mathbb{H}$ is considered as a quadrivariate function of the quaternion argument itself together with its three quaternion involutions, as seen in Section 2.1; namely, $f(q) = f(q, \overline{q}^{\boldsymbol{i}}, \overline{q}^{\boldsymbol{j}}, \overline{q}^{\boldsymbol{k}})$. The resulting quaternion widely linear model is

$$\mathbf{y} = \mathbf{u}^T\mathbf{x} + \mathbf{v}^T\overline{x}^{\boldsymbol{i}} + \mathbf{g}^T\overline{x}^{\boldsymbol{j}} + \mathbf{h}^T\overline{x}^{\boldsymbol{k}}. \tag{2.44}$$

By using the quaternion gradient defined in [24], the update equation of the quaternion WL-LMS coefficients becomes

$$\mathbf{w}^a(n+1) = \mathbf{w}^a(n) + \mu(2e^a(n)\mathbf{x}^{a^*}(n) - \mathbf{x}^{a^*}(n)e^{a^*}(n)). \tag{2.45}$$

where

$$\mathbf{w}^a = [\mathbf{u}^T\, \mathbf{v}^T\, \mathbf{g}^T\, \mathbf{h}^T], \tag{2.46}$$

$$\mathbf{x}^{a^*} = [\mathbf{x}^T\, \overline{\mathbf{x}}^{\boldsymbol{i}T}\, \overline{\mathbf{x}}^{\boldsymbol{j}T}\, \overline{\mathbf{x}}^{\boldsymbol{k}T}]^T, \tag{2.47}$$

$$e^a(n) = d(n) - \mathbf{w}^{a^T}(n)\mathbf{x}^a(n). \tag{2.48}$$

2.2 Dual-polarized quaternion OFDM

In this section, we briefly review the quaternion OFDM dual-polarized system, as first proposed by Meloni [42]. In that work, the author used both quaternion and hypercomplex commutative algebras to perform Fourier transforms. As a result, it was demonstrated that there is no difference in terms of BER performance between both quaternion and HCA schemes, nor by choosing different hypercomplex units as axes for the transforms.

OFDM is based on the discrete Fourier transform. For the quaternion OFDM scheme, [42] proved that the quaternion Fourier pair shown in (2.37) and (2.38) is suitable for this modulation technique. The quaternion OFDM transmitter system is illustrated in Figure 2.3. In general, a forward error correction code can be applied to the binary sequence. Other important modules used in OFDM schemes, such as carrier and frame synchronizers, and time and frequency interleaving, can be included as needed. Particularly, time and frequency synchronization for QOFM was a principal research topic of this thesis and will be approached in Chapter 3.

At the transmitter input of Figure 2.3, a serial-to-parallel conversion block stores N samples for computing the inverse Fourier transform.

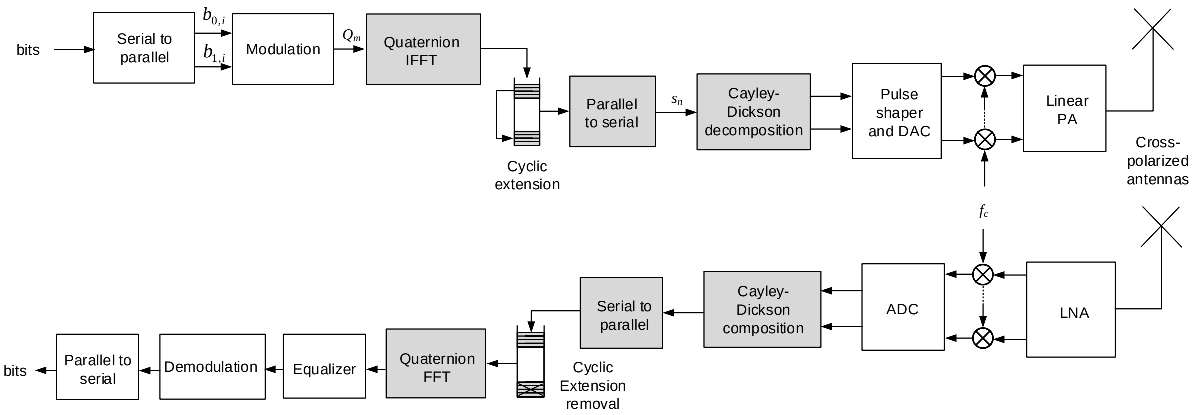

Figure 2.3 – Quaternion OFDM transmitter and receiver.

The quaternion symbol Q_m results from the CD form, with $\boldsymbol{\mu} = \boldsymbol{j}$ axis, i.e.,

$$Q_m = Q_{m,1} + Q_{m,2}\boldsymbol{j}, \tag{2.49}$$

where $Q_{m,1}$ and $Q_{m,2}$ are complex symbols belonging to $\mathbb{C}_i$. Incoming bit-streams are separated into two groups $b_{0,i}$ and $b_{1,i}$, for $0 \leq i \leq N_b - 1$; each of these groups defines an independent constellation, such that the compound constellation has 2^{2N_b} entries [42]. In the same way as complex OFDM, it is possible to use different digital modulation schemes (such as QPSK, 16QAM, and others) for different subcarriers and for each complex component, according to specific reliability needs or channel conditions.

The quaternion IFFT block performs the inverse quaternion discrete Fourier transform. The left-sided version with axis $\mu = \boldsymbol{j}$ of (2.37) and (2.38) are used, which can be implemented efficiently using two classical fast Fourier transform on both simplex and perplex parts independently. Thus, the complexity of these algorithms, without regard to the Cayley-Dickson decomposition, is twice that of the classical Fourier transform.

The next block appends the cyclic prefix, which, as in the complex case, provides a guard interval that avoids inter-symbol interference (ISI) and it is also used for frame synchronization, as it will be shown in Chapter 3. By using the time-shifting property of the quaternion Fourier transform, any consecutive N samples of the OFDM symbol m could be used; however, the last symbols are better for combating ISI.

After cyclic extension, quaternion symbols are serialized and passed through CD decomposition block, which splits the quaternion symbols into a pair of complex symbols to be transmitted by each element of the cross-polarized antenna. The last blocks of the transmitter side are typical in wireless communications systems; these blocks consist of a pulse shaper, a digital-to-analog converter followed by a mixer, and a power amplifier.

At the receiver, a low noise amplifier (LNA) prepares the signal for down-conversion and analog-to-digital, and the first step is to compose the symplectic form using (2.49); next, data is buffered for performing the Fourier transform. First, cyclic extension is removed before applying the direct quaternion Fourier transform. The data equalization may be conducted in the Fourier domain, as illustrated in Figure 2.3, but it might be applied in the time domain as well. The symplectic decomposition is performed inside the hypercomplex demodulation block; thereafter, a classical demodulator can be used.

Even though the QOFDM scheme presented in Figure 2.3 exhibit similar computational when compared to classical dual-polarized OFDM, the new scheme allows processing both polarization signals as a unit, which, in turn, enable the use of compact notations and the development of new signal processing techniques for synchronization, equalization, among others.

2.2.1 Channel model

In [43], the authors demonstrated that dual-polarized signals can be represented using quaternions. Later, [14] presented a model for dual-polarized channels using a single quaternion gain, instead of a matrix of four complex elements. Even though this result allows us to describe the transmission in dual-polarized systems in a compact form, this model is restricted by a relationship between cross-polar gains that is not necessarily fulfilled in practice. Therefore, throughout the present thesis, we use the classical 2×2 channel model, namely,

$$H_m^{\times} = \begin{bmatrix} h_m^{11} & h_m^{12} \\ h_m^{21} & h_m^{22} \end{bmatrix}, \tag{2.50}$$

where each element is a complex channel gain, h_m^{11} and h_m^{22} for signals received with the same polarization, and h_m^{12} and h_m^{21} for cross-polar scatter. More detailed descriptions for link model can be found in [42], [21]. Although (2.50) refers to a flat fading model for each cross and copolar channel, the same equation can be extended to frequency selective fading channel by considering each h_m^{ij} term as a vector channel impulse response and performing the corresponding convolution operations.

In an ideal scenario, the cross-polar scatter terms h_m^{12} and h_m^{21} vanish, this condition is represented by the uncoupled matrix,

$$H_m^{\perp} = \begin{bmatrix} h_m^{\mathrm{h}} & 0 \\ 0 & h_m^{\mathrm{v}}. \end{bmatrix} \tag{2.51}$$

Nevertheless, in practice, there are two main mechanisms of depolarization that contribute to the appearance of the cross-polar interference terms. Namely, the imperfect cross-polar-isolation (XPI) that characterizes real antennas and the wave scattering along the propagation channel, represented as cross-polar ratio (XPR) [44]. The latter phenomenon can be effectively combated by using adaptive filtering algorithms in cross-polarization interference cancelation (XPIC) techniques. Therefore, in the search for simplicity, we only consider, for simulation, the imperfect cross-polar isolation of antennas at transmitting and receiving sides, modeled by matrices M_t and M_r, respectively, so that

$$H_m^{\times} = M_r H_m^{\perp} M_t, \tag{2.52}$$

and,

$$M_t = \gamma_t \begin{bmatrix} 1 & \sqrt{\chi_t} \\ \sqrt{\chi_t} & 1 \end{bmatrix} \quad , \quad M_r = \gamma_r \begin{bmatrix} 1 & \sqrt{\chi_r} \\ \sqrt{\chi_r} & 1 \end{bmatrix}, \tag{2.53}$$

where XPI, ordinarily expressed in dB, is defined as χ_t^{-1} and χ_r^{-1} at transmitting and receivinging sides, respectively, and γ_t and γ_r are power normalization factors, computed as

$$\gamma_t = \frac{\sqrt{2}}{1+\sqrt{\chi_t}} \quad \text{and} \quad \gamma_r = \frac{\sqrt{2}}{1+\sqrt{\chi_r}}. \tag{2.54}$$

Using the following notation, which makes use of the Cayley-Dickson decomposition, the transmitted quaternion symbol $Q_m = Q_{m,1} + Q_{m,2}\boldsymbol{\mu}$ can be represented as $[Q_{m,1}, Q_{m,2}]$, which are the simplex and perplex parts of Q_m. After symbol transmission over the cross-polarized link, defined by (2.52), the received quaternion symbol plus noise is $Y_m = Q_m H_m^{\times} + Z$, or, explicitly,

$$\begin{aligned} Y_m &= [Y_{m,1}, Y_{m,2}] \\ &= [Q_{m,1}, Q_{m,2}] H_m^{\times} + [Z_1, Z_2] \\ &= [(Q_{m,1} H_m^{\text{hh}} + Q_{m,2} H_m^{\text{vh}}), (Q_{m,1}\, H_m^{\text{hv}} + Q_{m,2} H_m^{\text{vv}})] \\ &+ \ [Z_1, Z_2], \end{aligned} \tag{2.55}$$

where Z_1 and Z_2 are complex additive noise sources with identical variance.

As is well known, although the multiple benefits of OFDM inherited by QOFDM, these schemes share also a high sensitivity to time and frequency errors, which can destroy orthogonality between carriers, a fundamental condition for detection. Hence, the next section shows the effects of time and frequency impairments on the QOFDM signal. Afterward, Chapter 3 will present the proposed synchronization techniques to deal with these impairments.

2.2.2 Effects of time and frequency impairments in QOFDM

In classical OFDM, the existence of a frequency mismatch between receiver and transmitter oscillators, modeled by the CFO ϵ, destroys orthogonality between subcarriers and produces intercarrier interference (ICI). The qualitative effects of this frequency impairment on the interference level and over the overall performance are studied in [2] and [45], respectively. On the other hand, with regard to time synchronization, the receiver should guarantee the availability of N time samples to recover the frequency domain symbol by use of Fourier transform. Therefore, the operation window in which a time offset is allowed is equivalent to the difference between the cyclic prefix time and the duration of the channel response.

A similar analysis to the one presented in [2] can be easily performed using Eqs. (2.37) and (2.38), with the result that both time and frequency impairment sensitivity are also presented in the new QOFDM scheme.

2.3 Quaternion coding for MIMO

This section shows the main techniques available in the literature to construct quaternion orthogonal space-time block codes (QOSTBC), also called quaternion orthogonal designs (QOD).

2.3.1 Introduction

Space-time block codes (STBC) are derivations of Alamouti's code [46] first introduced by Tarok et al. [47] used to exploit combinations of space, time, and frequency diversity in MIMO systems over fading channels. The fundamental idea behind STBC is to send copies of a constellation symbol through a number of transmit antennas over different time-slots or carriers, providing transmission with a diversity gain comparable to legacy schemes of maximal-ration receive combining (MRRC), where multiple copies of the same signal are received and combined in a set of antennas in the receiving side to perform joint detection. The design of STBCs was largely studied in the literature for real and complex constellations. Nevertheless, the quaternion case has only been focused more recently in [15]. The following sections present the definition of orthogonal designs over real, complex, and quaternion constellations, as well as briefly review some techniques to find them out both from scratch and using known designs as building blocks.

2.3.2 Orthogonal designs

A real orthogonal design (ROD) of order n and type $\{s_1, s_2, ..., s_p\}$, denoted $OD(n, s_1, s_2, .., s_p)$, on real variables $x_1, x_2, ...x_p$, is an order n square matrix which entries are in the set $\{0, \pm x_1, \pm x_2, ..., \pm x_p\}$ that verifies

$$AA^T = \Big(\sum_{h=1}^{p} s_h x_h^2\Big) I_n. \tag{2.56}$$

Some examples of ROD are

$$D_1 = \begin{bmatrix} x_1 & x_2 \\ -x_2 & x_1 \end{bmatrix}, \ D_2 = \begin{bmatrix} x_1 & x_2 & x_3 & x_4 \\ -x_2 & x_1 & -x_4 & x_3 \\ -x_3 & x_4 & x_1 & -x_2 \\ -x_4 & -x_3 & x_2 & x_1. \end{bmatrix}. \tag{2.57}$$

which are $OD(2,1,1)$ and $OD(4,1,1,1,1)$, respectively. From the communication perspective, each row of these matrices represents a symbol time slot (STS), and each column represent the symbols sequentially transmitted by each antenna. Also, p is the number of transmitted symbols during the transmission of one block. The code rate of an OD is defined as the number of transmitted symbols by time slot unit, i.e.,

$$R = \frac{p}{n}. \tag{2.58}$$

A complex orthogonal design (COD) of order n and type $\{s_1, s_2, ..., s_p\}$ on complex variables $z_1, z_2, ...z_p$, denoted $COD(n, s_1, ..., s_p)$, is a square matrix with entries in the set $\{0, \pm z_1, \pm z_1^*, \pm z_2, \pm z_2^* ..., \pm z_p, \pm z_p^*\}$ that verifies

$$AA^H = \Big(\sum_{h=1}^{p} s_h |z_h^2|\Big) I_n. \tag{2.59}$$

Also, a COD on real variables $x_1, x_2, ...x_p$ and type $\{s_1, s_2, ..., s_p\}$ is a square matrix with entries in the set $\{0, \pm x_1, \pm \boldsymbol{i} x_1, \pm x_2, \pm \boldsymbol{i} x_2 ..., \pm x_p, \pm \boldsymbol{i} x_p\}$ satisfying

$$AA^H = \Big(\sum_{h=1}^{p} s_h x_h^2\Big) I_n. \tag{2.60}$$

The matrices

$$D_3 = \begin{bmatrix} z_1 & z_2 \\ -z_2^* & z_1^* \end{bmatrix}, \ D_4 = \begin{bmatrix} x_1 & x_2\boldsymbol{i} \\ x_2\boldsymbol{i} & x_1 \end{bmatrix} \tag{2.61}$$

are examples of $COD(2,1,1)$ on complex and on real variables, respectively. Particularly, D_3 is the well-known Alamouti's code [46].

A quaternion orthogonal design (QOD) on quaternion variables $q_1, q_2, ...q_u$ is an orthogonal matrix with elements in the set $\{0, \pm q_1, \pm q_1^*, \pm q_2, \pm q_2^* ..., \pm q_u, \pm q_u^*\}$ that satisfies

$$A^Q A = \Big(\sum_{h=1}^{u} s_h |q_h|^2\Big) I_n, \tag{2.62}$$

where $(.)^Q$ stands for transpose quaternion conjugate operation. It is also allowed right or left multiplication of the entries of A by quaternion numbers.

The fact that $A^Q A$ is diagonal ensures the transmitted signals are uncorrelated at the receiver. An orthogonal design that has entries that are linear combinations of the permitted variables of the respective sets is said to be a design that performs *linear processing*. Calderbank *et al.* proposed a quaternion-based QOD [48], but it was not with linear processing.

A classical result by Radon [49] establishes the existence of orthogonal designs only for square matrices with dimensions 2, 4, and 8. Although this result was derived for real matrices, Tarokh [47] extended it to complex as well as non-square matrices. Therefore, for an $r \times n$ matrix, the maximum diversity gain, i.e., the transmission power reduction allowed by the diversity scheme to achieve the same level of reliability compared to a single non-diversity transmission [50], is rn, which is achieved when the matrix is full-rank. In general, for an m-rank matrix of order $r \times n$, the diversity gain is mn [47]. Also, for $r \times n$ matrices, the code rate is $R = \dfrac{p}{r}$.

Analogously to the complex case, it is possible to define QODs on real or on complex variables. Therefore, many methods of construction of CODs from RODs can be applied to produce QODs starting from RODs or CODs.

2.3.3 Construction techniques based in real or complex orthogonal designs

A number of techniques are inspired or make use of ROD as well as COD, some of them are explained in this section.

2.3.3.1 Quaternion permutation matrices

A quaternion permutation matrix M is an n-order square matrix with exactly one non-zero element per row and per column, which verifies $M^Q M = M M^Q = I_n$. By using quaternion permutation matrices and OD or CODs, it is possible to produce QOD's through the following theorem [15].

Theorem 1. *Let D be an $r \times n$ ROD or COD of type $(s_1, s_2, ..., s_u)$ and let M and N quaternion permutation matrices of order $r \times r$ and $n \times n$, respectively. Then MDN is an $r \times n$ QOD of type $(s_1, s_2, ..., s_u)$.*

Example 2.3.1. Let the Alamouti's code, $D_3 = \begin{bmatrix} z_1 & z_2 \\ -z_2^* & z_1^* \end{bmatrix}$, and the quaternion permutation matrices $M = \begin{bmatrix} 0 & \boldsymbol{k} \\ \boldsymbol{i} & 0 \end{bmatrix}$, and $N = I_2$. By using Theorem 1, the matrix $Q_1 = MD_3N = \begin{bmatrix} -\boldsymbol{k}z_2^* & \boldsymbol{k}z_1^* \\ \boldsymbol{i}z_1 & \boldsymbol{i}z_2 \end{bmatrix}$, with $z_1, z_2 \in \mathbb{C}_i$, is a QOD.

The above technique for developing QODs is very powerful, due to its simplicity and the broad availability of real and complex ODs.

2.3.3.2 Symmetric-paired designs

Two CODs are said to be symmetric-paired if AB^H is symmetric and/or if $A^H B$ is symmetric. The following theorem provides a method to produce a QOD from two symmetric-paired CODs.

Theorem 2. *Let A and B, COD of type $(n, n, s_1, s_2, ..., s_u)$ and $(n, n, t_1, t_2, ..., t_u)$, respectively, on complex variables $z_1, z_2, ..., z_u$. If $A^H B$ is symmetric, then $A + B\boldsymbol{j}$ is a QOD of type $(n, n, s_1 + t_1, s_2 + t_2, ..., s_u + t_u)$ on complex variables $z_1, z_2, ..., z_u$.*

Example 2.3.2. A simple way to produce symmetric-paired CODs is by permutation of columns of a COD [51]. For example, it is straightforward that $D_3 = \begin{bmatrix} z_1 & z_2 \\ -z_2^* & z_1^* \end{bmatrix}$, and $D_5 = \begin{bmatrix} z_2 & z_1 \\ z_1^* & -z_2^* \end{bmatrix}$ are symmetric paired. Thus, $Q_2 = D_3 + D_5\boldsymbol{j} = \begin{bmatrix} z_1 + z_2\boldsymbol{j} & z_2 + z_1\boldsymbol{j} \\ -z_2^* + z_1^*\boldsymbol{j} & z_1^* - z_2^*\boldsymbol{j} \end{bmatrix}$ is a QOD. If we consider $q = z_1 + z_2\boldsymbol{j}$, then Q_2 can be rewritten as $\begin{bmatrix} q & -\boldsymbol{i}q\boldsymbol{k} \\ -\boldsymbol{k}q\boldsymbol{i} & -\boldsymbol{k}q\boldsymbol{k} \end{bmatrix}$

As seen in Examples 2.3.1 and 2.3.2, real and complex OD allow us to easily produce QOD. Nonetheless, in both cases, we move from a full rate complex code to half rate quaternion codes. Thus, techniques based in real or complex OD result in QOD with limited performance when compared with the original designs.

2.3.4 Construction techniques of quaternion codes.

2.3.4.1 Quaternion commuting variables

Two quaternion variables **a** and **b** are said to quaternion-commute if $ab^* = ba^*$. The use of a quaternion-commuting pair allows us to produce QOD by replacing complex variables with quaternions and making some adjustments. Some examples are $\begin{bmatrix} a & b \\ b & -a \end{bmatrix}$ or $\begin{bmatrix} a & \boldsymbol{j}b \\ \boldsymbol{i}b & -\boldsymbol{k}a \end{bmatrix}$. These QODs have their code rate limited by the restriction of a and b to be quaternion-commuting.

2.3.4.2 Amicable designs

Real OD, A and B are said to be amicable if $AB^T = BA^T$[52]. The existence of amicable designs was studied in [53], and they were used to build COD in [54]. Also, A and B are said to be complex amicable designs if $AB^H = BA^H$; and are said to be quaternion amicable designs if $AB^Q = BA^Q$. Although, [15] shows an example of a pair of quaternion amicable designs, the question of its existence and constructions remains open.

As seen in the previous sections, the use of ODs and CODs to develop QODs exhibits simplicity at the cost of limited performance. On the other hand, a full quaternion approach demands the existence of some mathematical relationships between the quaternion variable, which also compromises the code rate. Thus, the search for efficient QOD construction methods is an ongoing study.

Another research topic is the construction of QOD for a high number of antennas, i.e., with high dimensions. A classic approach uses small designs as building blocks for higher-dimension matrices. Among them, the quaternion coordinate interleaved orthogonal design is explained below.

2.3.5 Quaternion coordinate interleaved orthogonal designs

The so-called coordinate interleaved orthogonal design (CIOD) was generalized to quaternions in [55]. Through this technique, a $4n \times 4m$ QOD can be built based on any known $n \times m$ QOD, by using the structure

$$Q = \begin{bmatrix} \Theta_1(\tilde{q}_0, ..., \tilde{q}_{K/4-1}) & 0 & 0 & 0 \\ 0 & \Theta_2(\tilde{q}_{K/4}, ..., \tilde{q}_{2K/4-1}) & 0 & 0 \\ 0 & 0 & \Theta_3(\tilde{q}_{K/2}, ..., \tilde{q}_{3K/4-1}) & 0 \\ 0 & 0 & 0 & \Theta_4(\tilde{q}_{3K/4}, ..., \tilde{q}_{K-1}) \end{bmatrix}, \tag{2.63}$$

where the original quaternion variables are $q_i = \alpha_i + \beta_i \boldsymbol{i} + \gamma_i \boldsymbol{j} + \delta_i \boldsymbol{k}$, $i = 0, ..., K-1$, with $mod(K, 4) = 0$, and the interleaved variables q_i are obtained through an appropriate combination of components of 4 equally-spaced q_i's. Namely, $\tilde{q}_i = \alpha_i + \beta_{mod(i+K/4,K)} \boldsymbol{i} + \gamma_{mod(i+K/2,K)} \boldsymbol{j} + \delta_{mod(i+3K/4,K)} \boldsymbol{k}$; and the corresponding Θ_J, $J = 1, ..., 4$ are $n \times m$ QODs, which can even be the same.

As an example, consider the matrix $Q = \begin{bmatrix} p & q \\ q^* & -p^* \end{bmatrix}$, which is the Alamouti QOD over commuting variables p and q. Then, the matrix

$$\begin{bmatrix} \tilde{q}_0 & \tilde{q}_1 & 0 & 0 & 0 & 0 & 0 & 0 \\ \tilde{q}_1^* & -\tilde{q}_0^* & 0 & 0 & 0 & 0 & 0 & 0 \\ 0 & 0 & \tilde{q}_2 & \tilde{q}_3 & 0 & 0 & 0 & 0 \\ 0 & 0 & \tilde{q}_3^* & -\tilde{q}_2^* & 0 & 0 & 0 & 0 \\ 0 & 0 & 0 & 0 & \tilde{q}_4 & \tilde{q}_5 & 0 & 0 \\ 0 & 0 & 0 & 0 & \tilde{q}_5^* & -\tilde{q}_4^* & 0 & 0 \\ 0 & 0 & 0 & 0 & 0 & 0 & \tilde{q}_6 & \tilde{q}_7 \\ 0 & 0 & 0 & 0 & 0 & 0 & \tilde{q}_7^* & -\tilde{q}_6^*, \end{bmatrix} \tag{2.64}$$

where

$$\tilde{q}_0 = \alpha_0 + \beta_2 \boldsymbol{i} + \gamma_4 \boldsymbol{j} + \delta_6 \boldsymbol{k} \tag{2.65}$$
$$\tilde{q}_1 = \alpha_1 + \beta_3 \boldsymbol{i} + \gamma_5 \boldsymbol{j} + \delta_7 \boldsymbol{k} \tag{2.66}$$
$$\tilde{q}_2 = \alpha_2 + \beta_4 \boldsymbol{i} + \gamma_6 \boldsymbol{j} + \delta_0 \boldsymbol{k} \tag{2.67}$$
$$\tilde{q}_3 = \alpha_3 + \beta_5 \boldsymbol{i} + \gamma_7 \boldsymbol{j} + \delta_1 \boldsymbol{k} \tag{2.68}$$
$$\tilde{q}_4 = \alpha_4 + \beta_6 \boldsymbol{i} + \gamma_0 \boldsymbol{j} + \delta_2 \boldsymbol{k} \tag{2.69}$$
$$\tilde{q}_5 = \alpha_5 + \beta_7 \boldsymbol{i} + \gamma_1 \boldsymbol{j} + \delta_3 \boldsymbol{k} \tag{2.70}$$
$$\tilde{q}_6 = \alpha_6 + \beta_0 \boldsymbol{i} + \gamma_2 \boldsymbol{j} + \delta_4 \boldsymbol{k} \tag{2.71}$$
$$\tilde{q}_7 = \alpha_7 + \beta_1 \boldsymbol{i} + \gamma_3 \boldsymbol{j} + \delta_5 \boldsymbol{k} \tag{2.72}$$

is the quaternion CIOD in variables, $q_i = \alpha_i + \beta_i \boldsymbol{i} + \gamma_i \boldsymbol{j} + \delta_i \boldsymbol{k}$, $i = 0, ..., 7$.

2.4 Conclusions

This chapter presented a concise theoretical review of quaternion algebra, necessary to understand the ongoing developments and simulations. For an introduction to hypercomplex number systems, the readers can refer to [56], and for a comprehensive treatment of quaternions and their properties, we recommend Ward's book [57]. Also, [30] exhibits the theory of Fourier transform from a practical perspective, with special focus on image processing.

In this chapter, it was also presented a brief review of QOFDM, as proposed in [1]; special attention was put on its high sensitivity to time and frequency impairments, a well-known issue of OFDM that remains valid in its quaternion extension.

Besides, some techniques to design quaternion codes at the literature for implementation of space-time-polarization diversities in MIMO systems were presented. There, we included techniques based on existing real and complex designs, and also methods to produce high-order quaternion designs by using smaller ones as building blocks.

The latter two areas, QOFDM synchronization, and quaternion MIMO systems, were the main areas where the present research work made its contributions.

The next chapter focuses on demonstrating new algorithms for QOFDM synchronization based on existing techniques found in the literature.

3 Synchronization techniques for QOFDM

Over the past decades, OFDM was successfully applied in several wireless technologies such as Wi-Fi, and 5G mobile communications, among others. The main advantages of OFDM are its efficient use of radio-frequency spectrum, and its robustness against frequency selective fading and inter-symbol interference (ISI), among others. Nevertheless, OFDM relies on mutual orthogonality between subcarriers and this attribute makes it highly sensitive to synchronization impairments both in time and in carrier frequency, which demands the use of precise synchronization techniques. This drawback is inherited by dual-polarized QOFDM due to homomorphism between QFT and FT. However, as shown in this chapter, classic techniques for OFDM synchronization can be successfully reformulated to the hypercomplex scenario.

In this chapter, we present a brief review of the synchronization problem in QOFDM inherited from complex OFDM. Then, we introduce the quaternion reformulation of classical techniques for OFDM synchronization to the quaternion case, for both data-aided and non-data-aided cases. A new and elegant expression for STO CRLB is derived. Finally, the performance of these methods is evaluated through Monte Carlo simulations and some considerations are highlighted.

3.1 Synchronization techniques based on cyclic prefix

3.1.1 Reformulation of Van de Beek algorithm

The synchronization technique based on cyclic prefix for complex OFDM was proposed by [58, 59], which uses the periodicity of the cyclic prefix to jointly estimate the STO as well as CFO. This section extends this technique to quaternion OFDM resulting in an improved synchronization algorithm for DP-OFDM. The simplex and perplex parts of the n-th quaternionic sample to transmit s_n, respectively $s_{n,1}$ and $s_{n,2}$, may be considered i.i.d. random variables. These components come from an inverse quaternion Fourier transform, which can be decomposed into two sums of N complex symbols weighted by orthogonal basis functions. Therefore, for N large enough according to the central limit theorem, each of these components has a normal distribution. Moreover, the CD composition of independent complex random variables with normal distribution has also normal distribution.

For easing the mathematical development, a non-dispersive AWGN channel and ideal discrimination polarization paths with unitary gain are considered. Therefore, the effect of time and frequency impairments between transmitter and receiver sides allows modeling the received signal as

$$y_n = e^{i2\pi\epsilon n/N}\, s_{n-\delta} + z_n, \tag{3.1}$$

where δ is the integer symbol time offset (STO) and ϵ the carrier frequency offset (CFO) in the receiver and z_n is additive proper white Gaussian noise. As it is considered that the complex components of the quaternion s_1 and $s_2 \in \mathbb{C}_i$, the exponential factor on the right side of (3.1) should be applied by the left of the quaternion delayed symbol $s_{n-\delta}$ so that it introduces the same carrier frequency offset over both components.

At the receiver side, $L = 2N + N_c$ consecutive quaternion samples are observed forming a vector $\mathbf{y} = [y_0, y_1, ..., y_{L-1}]^T$. Non-italic is used for vector containing all samples in the observation interval. Inside this sequence, there is exactly one quaternion OFDM symbol that begins at unknown index δ, as illustrated in Figure 3.1.

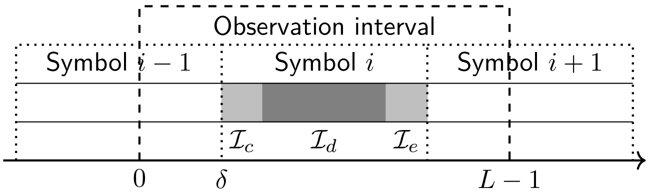

Figure 3.1 – Observation interval for synchronization based on cyclic prefix.

From Figure 3.1, sample sets containing cyclic prefix and the ending N_c samples of OFDM symbol are defined as

$$\begin{aligned} \mathcal{I}_c &\triangleq \{\delta,\ ...,\ \delta + N_c - 1\}, \quad \text{and} \\ \mathcal{I}_e &\triangleq \{\delta + N,\ ...,\ \delta + N + N_c - 1\}, \end{aligned}$$

whereas $\mathcal{I}_d$ stands for data samples. Notice that for $\forall n \in \mathcal{I}_c$,

$$\mathrm{E}[y_n y_{n+l}^*] = \begin{cases} \sigma_s^2 + \sigma_z^2 & \text{for } l = 0 \\ \sigma_s^2 e^{-i2\pi\epsilon} & \text{for } l = N \\ 0 & \text{otherwise,} \end{cases} \tag{3.2}$$

where $\sigma_s^2 = \mathrm{E}[|s_n|^2]$ and $\sigma_z^2 = \mathrm{E}[|z_n|^2]$ are the signal and noise variances, respectively.

The log-likelihood function for δ and ϵ parameters is

$$\Lambda(\mathbf{y}; \delta, \epsilon) \quad = \quad \log f(\mathbf{y}|\delta, \epsilon),$$

where f is the p.d.f. of $\boldsymbol{y}$.

If individual observations y_n's were statistically independent, f would be expressed as a multiplication of PDFs for individual observations. But according to (3.2), some samples are dependent, so by dropping the dependence on δ and ϵ at the PDFs for light notation, the log-likelihood function is

$$\Lambda(\mathbf{y};\delta,\epsilon) = \log\Bigg[\underbrace{\prod_{n\notin\{\mathcal{I}_c\cup\mathcal{I}_e\}} f(y_n)}_{\text{independent factors}} \underbrace{\prod_{n\in\mathcal{I}_c} f(y_n, y_{n+N})}_{\text{dependent factors}}\Bigg].$$

By taking now in the first product, all samples inside the observation interval, the above equation is

$$\Lambda(\mathbf{y};\delta,\epsilon) = \log\left[\prod_{\forall n} f(y_n) \prod_{n\in\mathcal{I}_c} \frac{f(y_n, y_{n+N})}{f(y_n)f(y_{n+N})}\right].$$

The joint PDF in the above equation is represented by a vector formed by a couple of samples $\boldsymbol{y} = [y_n, y_{n+N}]^T$, where here italic notation is used. We observe that the first factor in the above equation is independent of δ since the product is taken for any n, (in other words, for $\forall\delta$ the product is always the same), and independent of ϵ (since all four components of the quaternion are mutually independent), so that $\Lambda(\mathbf{y};\delta,\epsilon)$ is

$$\Lambda(\mathbf{y};\delta,\epsilon) = c_1 + \log\left[\prod_{n=\delta}^{\delta+N_c-1} \frac{f(\boldsymbol{y})}{f(y_n)f(y_{n+N})}\right], \tag{3.3}$$

by expressing now explicitly the limits in the second product and for any constant c_1. The PDFs needed in above equation are defined in (2.39) and (2.40).

By defining

$$\rho \triangleq \frac{\sigma_s^2}{\sigma_s^2+\sigma_z^2} = \frac{\text{SNR}}{\text{SNR}+1}, \tag{3.4}$$

the maximization of the log-likelihood function is shown at Section 3.1.3.1 to be

$$\Lambda(\mathbf{y};\delta,\epsilon) = \sum_{n=\delta}^{\delta+N_c-1} \mathcal{R}\{S(y_n y_{n+N}^*)e^{\boldsymbol{i}2\pi\epsilon}\} \\ -\frac{\rho}{2}(|y_n|^2 + |y_{n+N}|^2)]. \tag{3.5}$$

Finally, let

$$\gamma(l) \triangleq \sum_{n=l}^{l+N_c-1} \mathcal{S}\{y_n y_{n+N}^*\}, \tag{3.6}$$

$$\Phi(l) \triangleq \frac{1}{2}\sum_{n=l}^{l+N_c-1} (|y_n|^2 + |y_{n+N}|^2), \tag{3.7}$$

for $l = 1, 2, ..., M$, then (3.5) becomes

$$\Lambda(\mathbf{y};\delta,\epsilon) = |\gamma(\delta)|\cos(2\pi\epsilon + \angle\gamma(\delta)) - \rho\Phi(\delta). \tag{3.8}$$

For obtaining the values of δ and ϵ that maximize (3.8), it should be observed that ϵ only appears in the argument of the cosine function. Therefore, $\hat{\epsilon}$ is chosen in order to maximize the cosine function, that is,

$$\hat{\epsilon} = -\frac{1}{2\pi}\angle\gamma(\delta). \tag{3.9}$$

The $\hat{\delta}$ STO can be first obtained considering that $\hat{\epsilon}$ will be estimated by using the above equation at $\gamma(\hat{\delta})$, therefore from (3.8), it follows

$$\hat{\delta} = \arg\max_{\delta}[|\gamma(\delta)| - \rho\Phi(\delta)]. \tag{3.10}$$

It should be noted that although the estimation expressions have been derived by using quaternion algebra, an alternative implementation can be performed by using complex operations on the simplex and perplex parts of the received signal. In particular, (3.6) and (3.7) can also be calculated as

$$\gamma(l) \triangleq \sum_{n=l}^{l+N_c-1} (y_{n,1}\, y^*_{n+N,1} + y_{n,2}\, y^*_{n+N,2}), \tag{3.11}$$

$$\Phi(l) \triangleq \frac{1}{2} \sum_{n=l}^{l+N_c-1} (|y_{n,1}|^2 + |y_{n,2}|^2 + |y_{n+N,1}|^2 + |y_{n+N,2}|^2), \tag{3.12}$$

with homomorphic estimators in (3.9) and (3.10). These equations allow estimating the computation complexity of the proposed algorithm by comparing them with their corresponding counterparts in the classical algorithm. They also ease the practical implementation.

3.1.2 Simulation results

Monte Carlo (MC) simulations were performed to corroborate the theoretical development of OFDM timing and frequency offset estimation for single and dual-polarization antennas. For all conducted simulations, if not otherwise specified, the size of the FFT is $N = 256$, cyclic prefix size is $N_c = 64$, the number of virtual carriers is $N_v = 17$, modulation is QPSK, and AWGN channels are used. For fair result comparisons, the transmit power for SP and DP scenarios are the same, which means that for instance in the SP case if the transmit power is 1 W, this power is equally distributed per polarization in the dual case. The DP simulations use the quaternion OFDM scheme as presented in [42]. Moreover, simulation results are compared to theoretical CRLBs, as derived or reformulated in Section 3.1.3.

3.1.2.1 Symbol time offset

The simulation focuses on synchronization based on the cyclic prefix for both scenarios, single and dual polarization. The results are shown in Figure 3.2 for STO estimates. The number of MC simulation runs is 1×10^5 for SNR from -10 dB up to 20 dB, and from this value up to 30 dB is 1×10^6. The first remarkable observation is that the threshold effect is much better for the DP case in comparison to SP one, showing a difference of around 10 dB. On another note, as indicated in the theoretical development, the CRLB line for the DP case has double the slope of the SP case, which allows observing at SNR $= 20$ dB, a gain greater than one order of magnitude in the variance of the

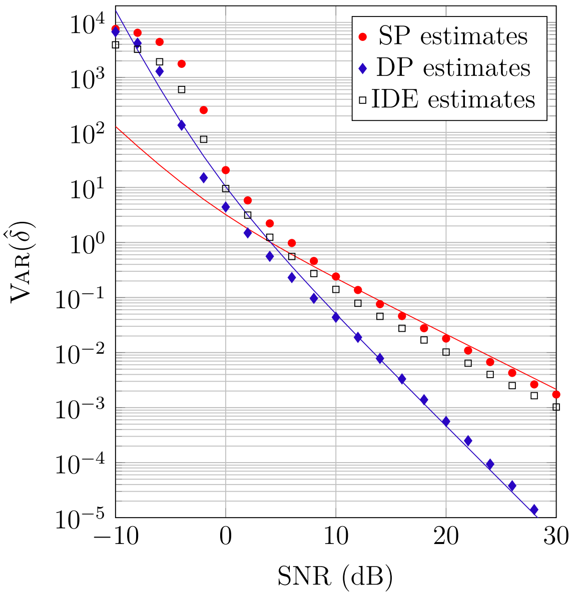

Figure 3.2 – Simulation results of SP and DP antennas systems: STO estimate variance versus SNR (dB) based on cyclic prefix approach, CRLBs are represented in continuous lines.

estimator. For comparison purposes, although somewhat unreal, the figure also includes the case of two independent-double estimate (IDE) for each of the channel pairs using complex-valued half-power signals OFDM modulated, where it is considered that both channels have the same gains, and they are submitted to the same time and frequency offsets. In this case, the average of two STO estimates is rounded to the near integer. The observed performance of this combined estimator, as expected, exhibits the same slope as the estimator of the SP case, as well as a performance gain of around 3 dB.

3.1.2.2 Carrier frequency offset

Results for CFO estimators are shown in Figure 3.3, where the number of MC runs is the same as in the previous case. The threshold effects for both cases are similar for CFO. Furthermore, as predicted by the theoretical development, 3 dB gain is noticed from DP over SP antenna systems. The average combined IDE real values of CFO show similar behavior to the DP case.

Although the above comparisons are fair in the sense that they use the same transmission power in both SP and DP cases, dual polarization systems use two low-noise amplifiers. A more conservative comparison would be considered to double the noise power in these scenarios, which means to displace the DP curves 3 dB to the right side. For instance, a vertical line at 10 dB for SP case would be compared to 7 dB-line of DP case. Even though the dual-slope line for log-variance versus SNR would still be better for STO estimates, CFO estimates will present similar behaviors.

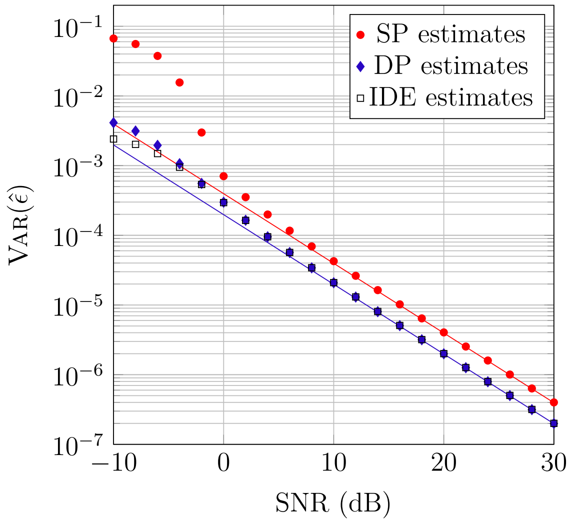

Figure 3.3 – Simulation results of SP and DP antenna systems for CFO estimator variances and CRLBs for cyclic prefix-based methods represented in continuous lines.

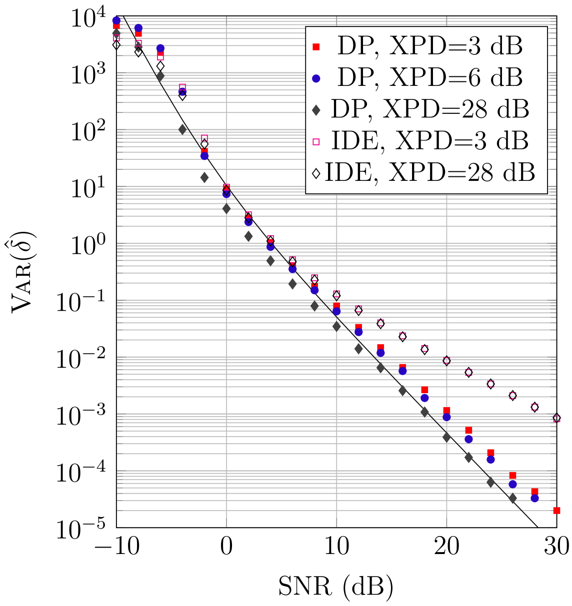

Figure 3.4 – Finite XPD for DP and IDE cases.

3.1.2.3 Finite XPD

The aim of this simulation is to show the performance of the estimators for finite cross-polarization discrimination (XPD). For this purpose, the channel model in (2.55) is applied. XPD is an overall parameter of the communication link, [21] which is set for direct and cross-polar paths to give the desired discrimination in dB without changing the transmit power. These real-valued parameters give the magnitude of the cross-polar discrimination parameters in (2.55) expressed in polar coordinates. Their phases are taken from a uniform random generator in the interval $(-\pi, \pi)$. These parameters remain fixed at each OFDM transmit symbol.

Figure 3.4 shows that systems of DP antennas are quite immune to the cross-polarization discrimination factor, even at 3 dB XPD. The reason for this fact is the time alignment of CP information (see Figure 3.1) at the direct and cross-polar paths. This fact is even more evident in the IDE case, where no discernible variations are observed.

3.1.3 Cramer-Rao lower bound

The Cramer-Rao lower bound on the error variance of parameter estimation is extensively used in engineering problems as a practical metric for the performance analysis of estimators. In order to simplify the STO CRLB derivation, a common practice in OFDM synchronization is firstly to estimate the STO considering no carrier offset, and afterward to perform the CFO estimation. This practice is justified by the fact that STO is based on the partial correlation of the received signals, in which the symbol samples are submitted to the same carrier offset. Therefore, here ϵ is considered zero. In [60], CRLB is derived by using pulse-shaped OFDM, which conducts to numerical methods for computing bounds. Here a different approach is applied based on computing the second derivative of the log-likelihood function. The CRLB for the STO estimate derived in Section 3.1.3.2 is

$$\textsc{Var}(\hat{\delta}) \geq \frac{1-\rho^2}{\rho^2(\frac{N-N_v}{N})}, \tag{3.13}$$

where N_v is the number of virtual sub-carriers (including DC sub-carrier). The variance of the product of the simplex and the perplex parts of random variables taken from these zero-mean independent random processes is equal to the product of respective variances. In the light of this observation, aiming to extend (3.13) for receivers of DP antennas, the following approximation holds:

$$\text{CRLB}[\hat{\delta}]_{\text{DP}} \simeq \left(\text{CRLB}[\hat{\delta}]_{\text{SP}}\right)^2. \tag{3.14}$$

A formal demonstration of this result is under study by the authors.

The CRLB of CFO estimates from DP antennas is derived in Section 3.1.3.3. Table 3.1 summarizes the CRLBs derived or reformulated for both STO and CFO estimates, as well as it includes CRLB for CP in [61].

Table 3.1 – Cramer-Rao lower bounds

CRLB	Ref.
$\text{CRLB}[\hat{\delta}]_{\text{SP}} \geq \dfrac{1-\rho^2}{\rho^2(\frac{N-N_v}{N})}$	(3.13)
$\text{CRLB}[\hat{\delta}]_{\text{DP}} \simeq (\text{CRLB}[\hat{\delta}]_{\text{DP}})^2$	(3.14)
$\text{CRLB}[\hat{\epsilon}]_{\text{SP}} \geq 1/(4\pi^2 N_c\,\text{SNR})$	[61]
$\text{CRLB}[\hat{\epsilon}]_{\text{DP}} \simeq \text{CRLB}[\hat{\epsilon}]_{\text{SP}}/2$	(3.36)

3.1.3.1 The log-likelihood function

By use of a property of quaternion conjugation and the interchangeability between conjugation and expected value operators, that is, $\mathrm{E}[y_{n+l}y_n^*] = (\mathrm{E}[y_n y_{n+l}^*])^*$, the covariance matrix for quaternion-valued samples is calculated as

$$\mathbf{K}_{\boldsymbol{y}} = (\sigma_s^2 + \sigma_z^2)\begin{bmatrix} 1 & \rho e^{-\boldsymbol{i}2\pi\epsilon} \\ \rho e^{\boldsymbol{i}2\pi\epsilon} & 1 \end{bmatrix}. \tag{3.15}$$

The joint PDF of the vector formed by a couple of samples $\boldsymbol{y} = [y_n, y_{n+N}]^T$ is obtained by substituting (3.15) into (2.39), which yields

$$f(y_n, y_{n+N}) = \frac{16}{\pi^4(\sigma_s^2+\sigma_z^2)^4(1-\rho^2)^2} \exp\left\{\frac{-2\left[|y_n|^2 + |y_{n+N}|^2 - 2\rho\mathcal{R}\{y_n^* e^{-\boldsymbol{i}2\pi\epsilon} y_{n+N}\}\right]}{(\sigma_s^2+\sigma_z^2)(1-\rho^2)}\right\}. \tag{3.16}$$

Besides, from (2.40), the PDF of y_n and y_{n+N} are

$$f(y_n) = \frac{4}{\pi^2(\sigma_s^2+\sigma_z^2)^2}\exp\Big(-\frac{2|y_n|^2}{\sigma_s^2+\sigma_z^2}\Big), \tag{3.17}$$

and

$$f(y_{n+N}) = \frac{4}{\pi^2(\sigma_s^2+\sigma_z^2)^2}\exp\Big(-\frac{2|y_{n+N}|^2}{\sigma_s^2+\sigma_z^2}\Big). \tag{3.18}$$

For $\mathbf{K}_{\boldsymbol{y}}$, PDFs in (2.39) and (2.40) are derived and substituted into (3.3), which after some algebraic manipulations gives

$$\Lambda(\mathbf{y};\delta,\epsilon) = c_1 + c_2\sum_{n=\delta}^{\delta+N_c-1}\Big[\mathcal{R}\{y_n^* e^{-\boldsymbol{i}2\pi\epsilon}y_{n+N}\} - \frac{\rho}{2}(|y_n|^2 + |y_{n+N}|^2)\Big], \tag{3.19}$$

where c_1 and c_2 are constants independent of δ and ϵ. Therefore, maximizing (3.19) is equivalent to maximizing only the sum of the right side of (3.19), that is,

$$\Lambda(\mathbf{y};\delta,\epsilon) = \sum_{n=\delta}^{\delta+N_c-1}[\mathcal{R}\{y_n^* e^{-\boldsymbol{i}2\pi\epsilon}y_{n+N}\} - \frac{\rho}{2}(|y_n|^2 + |y_{n+N}|^2)]. \tag{3.20}$$

In order to simplify the above equation, the identity

$$\mathcal{R}\{azb\} = \mathcal{R}\{\mathcal{S}\{a^*b^*\}z^*\}, \tag{3.21}$$

demonstrated in (2.8), is used.

3.1.3.2 CRLB for STO estimate

The CRLB for STO estimate is developed here using complex-valued samples and considering $\epsilon = 0$. The log-likelihood function, in this case, is [58]

$$\Lambda(\mathbf{y};\delta) = c_1 + c_2\Big[\mathcal{R}_e\{\gamma(\delta)\} - \rho\phi(\delta)\Big], \tag{3.22}$$

where c_1 and c_2 are constants independent of δ. Considering in (3.3) that the real and imaginary parts of y_n and y_{n+N} are independent, the latter constant explicitly is

$$c_2 = \frac{\rho}{2(\sigma_s^2+\sigma_z^2)(1-\rho^2)}. \tag{3.23}$$

The CRLB is determined by [62]

$$\textsc{Var}(\hat{\delta}) \geq \frac{1}{-\mathrm{E}[\frac{\partial^2\Lambda(\mathbf{y};\delta)}{\partial\delta^2}]}\ . \tag{3.24}$$

According to Lemma 2 below, the expected value of the log-likelihood has a triangular shape around $\hat{\delta}$, so that in the first derivative of $\Lambda(\mathbf{y};\delta)$ the constant c_1 vanishes, and therefore it has a bipolar pulse shape. The second derivative of the expression in brackets in (3.22) is proportional to the amplitude of this pulse at optimum δ, being equal to $-2[(N-N_v)/N]\sigma_s^2$, where N_v is the number of virtual sub-carriers. A simulation that illustrates this important result is conducted in Section 3.1.3.4 for easy understanding. This second derivative and (3.23) in (3.24) conducts to

$$\textsc{Var}(\hat{\delta}) \ \ \geq \frac{(1-\rho^2)(\sigma_s^2+\sigma_z^2)}{\rho(\frac{N-N_v}{N})\sigma_s^2},$$

and by using (3.4), the CRLB can be expressed as (3.13).

Lemma 2. The expected value of the log-likelihood function exhibits a triangular shape around δ at the optimum position for a displacement of α, that is,

$$\mathrm{E}[\Lambda(\mathbf{y};\delta+\alpha)] = -|\alpha|\sigma_s^2. \tag{3.25}$$

Proof. Let $\alpha > 0$, therefore

$$\mathrm{E}[\Lambda(\mathbf{y};\delta+\alpha)] = \mathrm{E}\Big[\mathcal{R}_e\Big\{\sum_{n=0}^{N_c-1} y_{n+\delta+\alpha}y^*_{n+N+\delta+\alpha}\Big\} - \frac{\rho}{2}\sum_{n=0}^{N_c-1}|y_{n+\delta+\alpha}|^2 + |y_{n+N+\delta+\alpha}|^2\Big]. \tag{3.26}$$

By splitting the first sum into two ones, it follows

$$\mathrm{E}[\Lambda(\mathbf{y};\delta+\alpha)] = \mathrm{E}\Big[\mathcal{R}_e\Big\{\sum_{n=0}^{N_c-1-\alpha} y_{n+\delta+\alpha}y^*_{n+N+\delta+\alpha} + \sum_{n=N_c-\alpha}^{N_c-1} y_{n+\delta+\alpha}y^*_{n+N+\delta+\alpha}\Big\}$$
$$- \frac{\rho}{2}\sum_{n=0}^{N_c-1}|y_{n+\delta+\alpha}|^2 + |y_{n+N+\delta+\alpha}|^2\Big]. \tag{3.27}$$

Observe that, being δ the initial index of $\mathcal{I}_c$ interval, all indexes of terms $y_{n+\delta+\alpha}$ in the first sum also $\in \mathcal{I}_c$, therefore

$$\begin{aligned}
\mathrm{E}\Big[\mathcal{R}_e\Big\{\sum_{n=0}^{N_c-1-\alpha} y_{n+\delta+\alpha}y^*_{n+N+\delta+\alpha}\Big\}\Big] &= \mathcal{R}_e\Big\{\sum_{n=0}^{N-1-\alpha}\mathrm{E}\Big[(s_{n+\delta+\alpha}+z_{n+\delta+\alpha})(s^*_{n+N+\delta+\alpha}+z^*_{n+N+\delta+\alpha})\Big]\Big\} \\
&= \mathcal{R}_e\Big\{\sum_{n=0}^{N_c-1-\alpha}\mathrm{E}[|s_{n+\delta+\alpha}|^2]\Big\} \\
&= (N_c-\alpha)\sigma_s^2, \qquad (3.28)
\end{aligned}$$

and that at the second sum, samples indexed $\in \mathcal{I}_d$, therefore $y_{n+\delta+\alpha}$ and $y_{n+N+\delta+\alpha}$ are independent. By applying (3.28) and (3.4) in (3.27), it gives

$$\mathrm{E}[\Lambda(\mathbf{y};\delta+\alpha)] = (N_c-\alpha)\sigma_s^2 - \frac{\rho}{2}\sum_{n=0}^{N_c-1}2\sigma_y^2 = -\alpha\sigma_s^2. \qquad (3.29)$$

Similarly, for $\alpha < 0$, it follows

$$\mathrm{E}[\Lambda(\mathbf{y};\delta+\alpha)] = \alpha\sigma_s^2,$$

which conducts to (3.25). $\square$

3.1.3.3 CRLB for CFO estimate

In order to derive the CRLB of the CFO estimates for the CP method, it is considered $\delta = 0$. In other words, the STO has been perfectly estimated and corrected prior to the CFO estimation, which can be achieved by applying one of the STO estimators. Thus, the received signal in (3.1) is modeled simply by

$$y_n = e^{i2\pi\epsilon n/N}s_n + z_n, \qquad (3.30)$$

where the quaternion-valued received samples can be limited to one OFDM symbol, i.e., $\mathbf{y} = [y_0, y_1, ..., y_{M-1}]^T$. The CRLB for the variance of any unbiased CFO estimator is lower bounded [62] by

$$\mathrm{V\small{AR}}(\hat{\epsilon}) \geq \frac{1}{-\mathrm{E}[\frac{\partial^2\Lambda(\mathbf{y};\epsilon)}{\partial\epsilon^2}]}, \qquad (3.31)$$

where $\Lambda(\mathbf{y};\epsilon) \triangleq \log f(\mathbf{y}|\epsilon)$ is the log-likelihood function of $\mathbf{y}$, given the true-value ϵ, whose calculation was derived in Section 3.1.1 for the joint ML estimation. Here as starting point, it is found the CRLB from (3.19), since c_1 is independent of ϵ, as well as it is the negative term in the inner summation, therefore

$$\frac{\partial^2\Lambda(\mathbf{y};\epsilon)}{\partial\epsilon^2} = c_2\frac{\partial^2}{\partial\epsilon^2}\Big[\sum_{m\in\mathcal{I}_c}\mathcal{R}\{y_m^*e^{-i2\pi\epsilon}y_{m+N}\}\Big] \qquad (3.32)$$

where $c_2 = 4\rho/[(\sigma_s^2 + \sigma_n^2)(1-\rho^2)]$, and ρ is defined in (3.4). In this way,

$$\begin{aligned}
\mathrm{E}[-\frac{\partial^2\Lambda(\mathbf{y};\epsilon)}{\partial\epsilon^2}] &= c_3 \sum_{m\in\mathcal{I}_c} \mathrm{E}[\mathcal{R}\{y_m^* e^{-i2\pi\epsilon} y_{m+N}\}] \\
&= c_3 \sum_{m\in\mathcal{I}_c} \mathrm{E}[\mathcal{R}\{\mathcal{S}(y_m y_{m+N}^*) e^{i2\pi\epsilon}\}] \\
&= c_3 \sum_{m\in\mathcal{I}_c} \mathcal{R}\{\mathcal{S}(\mathrm{E}[y_m y_{m+N}^*]) e^{i2\pi\epsilon}\},
\end{aligned} \tag{3.33}$$

where $c_3 = 4\pi^2 c_2$, and the second line was obtained by using the property (2.8). Also, from (3.2), $\mathrm{E}[y_m y_{m+N}^*] = \sigma_s^2 e^{-i2\pi\epsilon}$ for $m \in \mathcal{I}_c$, by substituting this and the expression of c_3 into (3.33), this gives

$$\mathrm{E}[-\frac{\partial^2\Lambda(\mathbf{y};\epsilon)}{\partial\epsilon^2}] = \frac{16\pi^2\rho^2 N_c}{1-\rho^2}, \tag{3.34}$$

which lead to the CRLB of the CFO estimate

$$\mathrm{V{\scriptsize AR}}(\hat{\epsilon}) \geq \frac{1-\rho^2}{16\pi^2\rho^2 N_c}. \tag{3.35}$$

As expected, this result shows 3 dB gain when compared to SP case [61]. Moreover, at high SNR $\frac{1-\rho^2}{\rho^2} \simeq \frac{2}{SNR}$. Therefore, it gives

$$\mathrm{V{\scriptsize AR}}(\hat{\epsilon}) > \frac{1}{8\pi^2 N_c \mathrm{SNR}}. \tag{3.36}$$

3.1.3.4 Estimate of log-likelihood function

For illustration purposes, Figure 3.5(a) shows an estimate of the log-likelihood function $\Lambda(\mathbf{y};\delta)$ by means of time averaging over 10,000 runs for a STO equal to 120 samples at SNR = 20dB for complex-valued signals. The number of virtual sub-carriers is 33, and all other simulation parameters are the same as the previous ones. One can observe that the log-likelihood function presents a triangular shape around the STO value, as shown in Section 3.1.3.2, Lemma 2. In order to verify the log-likelihood for a small symbol time offset, the simulations were conducted over interpolated signal by an oversampling factor of 32. This interpolation process uses the zero padding technique in the FFT domain [63]. The same behavior of the log-likelihood function is also noticed, exhibiting a triangular shape, as observed in the small panel in the figure. Figure 3.5(b) shows a time-averaging estimate of the 2nd-order central derivative of $\Lambda(\mathbf{y};\delta)$, where the minimum value is $-2[(N-N_v)/N]\sigma_s^2 = -1.742$, for unit signal variance. The small panel in the figure shows the 2nd-order central derivative of the over-sampled signal.

3.2 Synchronization techniques based on training symbols

Synchronization based on training sequence is used in OFDM systems operating at bursty packaged data using a frame structure. The method presented in this section

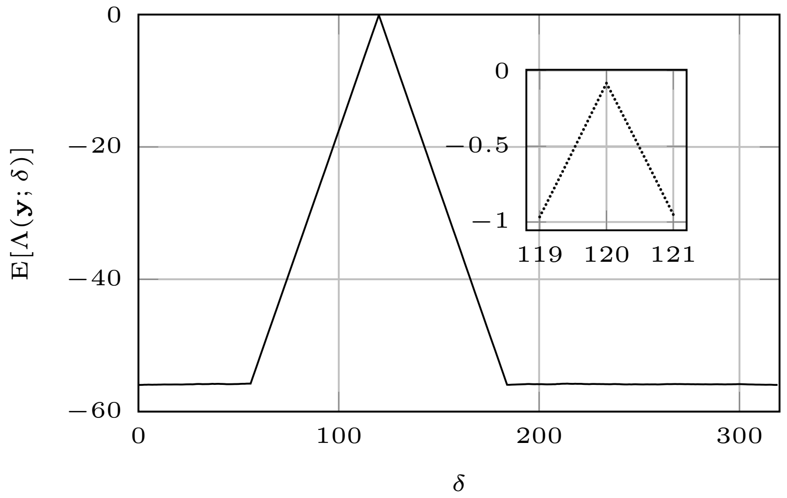

(a) (a)

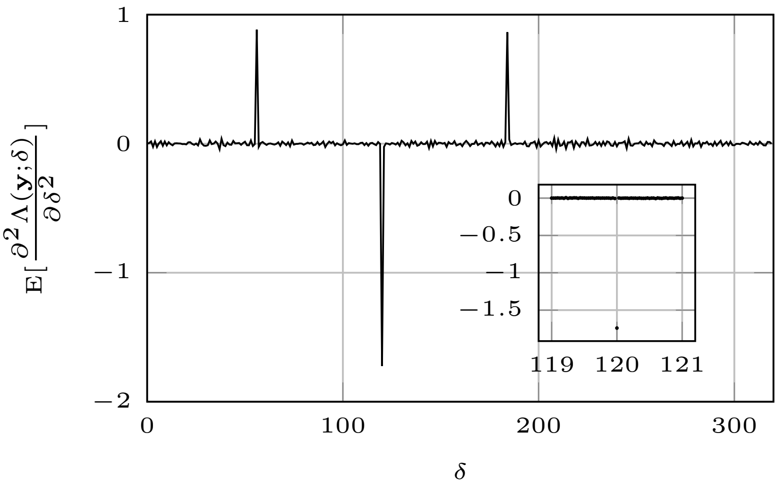

(b) (b)

Figure 3.5 – (a) Time-averaging estimate of $\Lambda(\mathbf{y};\delta)$. (b) Time-averaging estimate of the second-derivative of $\Lambda(\mathbf{y};\delta)$.

can be applied to find the start of the frame, as well as for carrier frequency offset (CFO) estimation by the use of training sequences present in one or more consecutive OFDM symbols.

3.2.1 Reformulation of Schimdl and Cox algorithm

The classic algorithm for complex OFDM using training symbols was proposed by Schimdl and Cox [64], which uses a periodic training sequence known as preamble, consisting of one or two OFDM symbols transmitted at the beginning of the frame. These training symbols are constructed so that, apart from the cyclic extension, they exhibit in the time domain two equal halves. For this purpose, it is possible to conceive these sequences by a pseudo-noise (PN) generator applied directly in the time domain, as well as in the frequency domain, where the PN sequence is transmitted at even sub-carrier frequencies, and zeros are placed at odd ones. Therefore, the inverse Fourier transform exhibits the desired symmetry in time. These training sequences are used to detect the frame start. It can also be used for refining CFO estimation, allowing fractional CFO, denoted by ϵ, where $\epsilon < 1$. The carrier frequency integer offset may be determined by using the second OFDM symbol. These training sequences have also an important role in fast channel response estimation, as for example in the case of IEEE 802.15.4, [65], where a long term field (LTF) is used for fast equalization and synchronization.

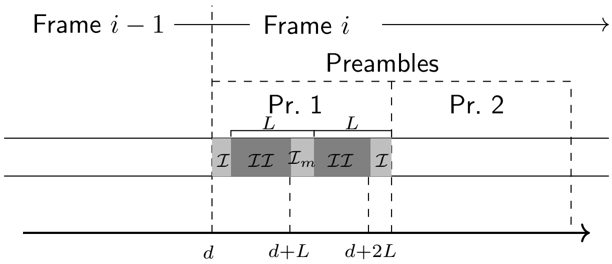

Figure 3.6 – Preamble sequence at frame beginning for synchronization based on training preamble, where middle samples $\mathcal{I}_m$ are identical to those of cyclic prefix $\mathcal{I}$.

The proposed method is based on the estimation of the partial autocorrelation function of the received sequence y_n. For that, let $L = N/2$, and $\mathcal{I}$ is the cyclic prefix range as illustrated in Figure 3.6. If the conjugate of a sample from the first half is multiplied by a sample at L samples apart, and considering that the channel response remains the same during an OFDM symbol, the effect of the channel should cancel, and the result will have phase $\pi\epsilon$.

By placing the training sequence quaternion samples $X_0, X_1, \ldots, X_{L-1}$ at even subcarriers of the quaternion OFDM symbol, the transmit symbols in time domain are

$$x_n = x_{n,1} + x_{n,2}\boldsymbol{j} = \frac{1}{N}\sum_{l=0}^{L-1} e^{\boldsymbol{i}2\pi n(2l)/N} X_l \tag{3.37}$$

for $n = 0,\ 1,\ \ldots,\ N-1$.

Consider initially an estimator, which will be justified in the sequence, computed for instant d sample-by-sample

$$\begin{aligned} P(d) &= \sum_{m=0}^{L-1} S\{r_{d+m} r^*_{d+m+L}\}, \\ R(d) &= \sum_{m=0}^{L-1} |r_{d+m+L}|^2, \end{aligned} \tag{3.38}$$

where $R(d)$ is used for normalization of $P(d)$. These equations may be computed recursively as

$$\begin{aligned} P(d+1) &= P(d) + S\{r_{d+L} r^*_{d+2L}\} - S\{r_d r^*_{d+L}\}, \\ R(d+1) &= R(d) + |r_{d+2L}|^2 - |r_{d+L}|^2. \end{aligned} \tag{3.39}$$

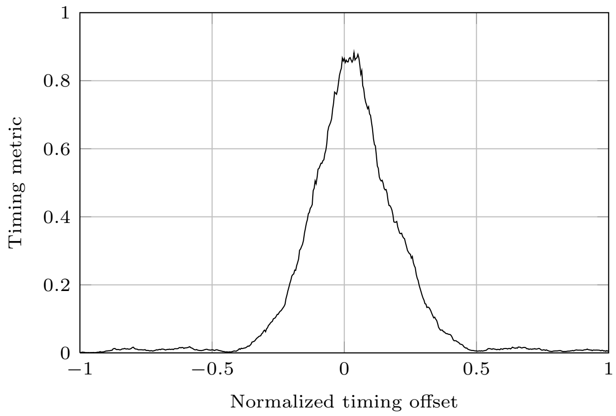

Figure 3.7 – Example of timing metric for synchronization based on training sequence (SNR = 10 dB).

Therefore, a time metric is defined as

$$M(d) = \frac{|P(d)|^2}{[R(d))]^2}. \tag{3.40}$$

This metric exhibits a plateau for values of index $d \in \mathcal{I}$, and a rising and falling time equal to $N/2$ as shown in Figure 3.7 for $N_c/N = 0.125$, where x-axis represents the symbol time offset (STO) normalized to the OFDM symbol duration. These results are similar to the complex technique [64].

A peak detector may be used for the STO estimation. Therefore, considering the quaternion OFDM symbol is already synchronized in time, the received signal for each polarization after removing the cyclic prefix is

$$r_{n,1} = y_{n,1} + z_{n,1}, \tag{3.41}$$

$$r_{n,2} = y_{n,2} + z_{n,2}, \tag{3.42}$$

where $z_{n,1}$ and $z_{n,2}$ are the AWGN components, so they are independent complex Gaussian variables with zero mean and variance $\sigma^2/2$. The signal components of $r_{n,1}$ and $r_{n,2}$ are, respectively,

$$\begin{aligned} y_{n,1} \quad &= \tfrac{1}{N}\textstyle\sum_{l=0}^{L-1} e^{i2\pi n(2l+\epsilon)/N} X_{l,1} H_{2l}^{11} \\ &+ \tfrac{1}{N}\textstyle\sum_{l=0}^{L-1} e^{\boldsymbol{i}2\pi n(2l+\epsilon)/N} X_{l,2} H_{2l}^{21} \end{aligned} \tag{3.43}$$

and

$$\begin{aligned} y_{n,2} \quad &= \tfrac{1}{N}\textstyle\sum_{l=0}^{L-1} e^{i2\pi n(2l+\epsilon)/N} X_{l,1} H_{2l}^{12} \\ &+ \tfrac{1}{N}\textstyle\sum_{l=0}^{L-1} e^{\boldsymbol{i}2\pi n(2l+\epsilon)/N} X_{l,2} H_{2l}^{22}. \end{aligned} \tag{3.44}$$

The CD compositions of these components give $r_n = r_{n,1} + r_{n,2}\boldsymbol{j}$, $z_n = z_{n,1} + z_{n,2}\boldsymbol{j}$, and $y_n = y_{n,1} + y_{n,2}\boldsymbol{j}$. Besides, we observe from (3.43) and (3.44) that

$$y_{n+L,1} = e^{\boldsymbol{i}\pi\epsilon} y_{n,1}, \tag{3.45}$$

$$y_{n+L,2} = e^{\boldsymbol{i}\pi\epsilon} y_{n,2}, \tag{3.46}$$

and therefore $y_{n+L} = e^{i\pi\epsilon} y_n$, for $n = 0, 1, ..., L-1$. As a consequence, it follows

$$r_n r_{n+L}^* = (y_n + z_n)(e^{i\pi\epsilon} y_n + z_{n+L})^* \tag{3.47}$$

$$= |y_n|^2 e^{-i\pi\epsilon} + y_n z_{n+L}^* + z_n y_n^* e^{-i\pi\epsilon} + z_n z_{n+L}^*. \tag{3.48}$$

When considering expected values in the above equation, it is evident that only the first term contains information about ϵ and, additionally, that the perplex component of this term is null. Furthermore, the last three terms represent noise components for estimation, and they have both simplex and perplex parts different from zero. Therefore, it is possible to suppress half of the noise components by taking only the simplex part of the terms in (3.48), i.e., the modified estimator for quaternion case results

$$\hat{\epsilon} = -\frac{1}{\pi} \angle P(\hat{d}), \tag{3.49}$$

where $P(d) = \sum_{n=0}^{L-1} S\{r_{d+n} r_{d+n+L}^*\}$ is evaluated at the optimum index $\hat{d}$ inside the CP interval $\mathcal{I}$, as shown in Figure 3.6. As can be observed from the above equation, the CFO estimator range is the interval $(-1, 1)$ times the frequency resolution, for $P(\hat{d})$ argument in $(-\pi, \pi)$ range.

The Cramer-Rao lower bound (CRLB) of the above estimator is derived in Section 3.2.3, which shows a gain of 3 dB of the CFO estimator variance when compared to the complex counterpart.

As a final remark, one observes that the metrics $P(d)$, $R(d)$, and therefore $M(d)$ can be expressed in terms of simplex and perplex parts of the observed signal, namely:

$$\begin{aligned} P(d) &= \sum_{m=0}^{L-1} (r_{d+m,1} r_{d+m+L,1}^* + r_{d+m,2} r_{d+m+L,2}^*), \\ R(d) &= \sum_{m=0}^{L-1} (|r_{d+m+L,1}|^2 + |r_{d+m+L,2}|^2), \end{aligned} \tag{3.50}$$

using only complex algebra. Therefore, we can observe that the use of quaternion algebra has conducted to the derivation of a new improved synchronization algorithm that can be implemented by the use of only complex-valued variables.

3.2.2 Simulation results

The algorithm presented for carrier frequency offset estimation was simulated for dual-polarized quaternion OFDM and compared to single-polarized complex OFDM, considering only an ideal dual-polarization link model of the channel without cross-polarization interference. For all conducted simulations, $N = 256$ was used as the size of the FFT, and cyclic prefix size was $N_c = 64$; for a total of 10^5 iterations performed for each case. For a fair comparison, the power transmission used for each element of the orthogonally polarized antenna of the quaternion case is half the power transmitted over the unique antenna of the complex case, setting the same irradiated power of the complex

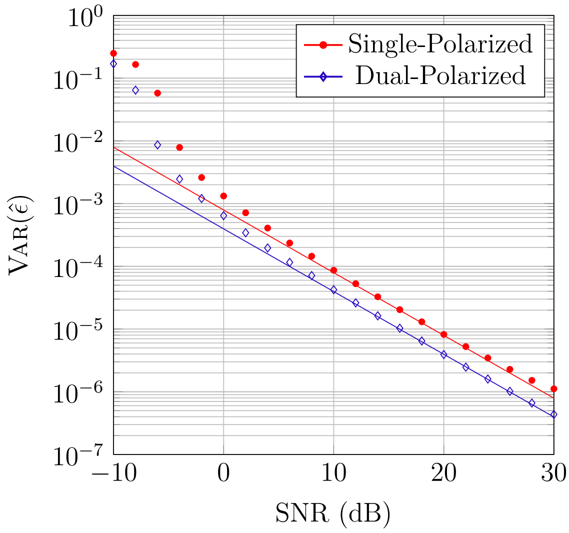

Figure 3.8 – CFO estimator variance compared to SP case.

case. A total of 10^4 frames is transmitted in each case over the same AWGN channel. All conducted simulations use quaternion OFDM as in [42].

Simulation results are shown in Figure 3.8, where continuous lines correspond to theoretical CRLBs, according to Table 3.1. In this simulation, we used only one preamble symbol for estimating the fractional part of the CFO. Results show a 3 dB gain of estimator variance when quaternions are compared to single-polarized OFDM [64]. This performance improvement is attributed to diversity gain resulted from using dual-polarization transmissions.

3.2.3 Cramér-Rao lower bound

In [64], authors showed that a CFO estimator obtained by partial correlation in time domain, as the one derived in (3.49), is the maximum-likelihood estimator (MLE), and consequently attains the CRLB at high signal to noise ratio (SNR). Thus, appealing to the isomorphism between complex and quaternion estimators, one can conclude that the proposed estimator also attains its corresponding CRLB under the same condition. In order to obtain the variance of the proposed estimator, the method in [2] is used. It should be noted that $P(\hat{d}) \in \mathbb{C}_i$ is a complex number with angle $-\pi\hat{\epsilon}$, so the rotated complex $P(\hat{d})e^{i\pi\epsilon}$ has $\arg(P(\hat{d})e^{i\pi\epsilon}) = -\pi\hat{\epsilon} + \pi\epsilon = -\pi(\hat{\epsilon} - \epsilon)$, from which the estimation error is derived as

$$\hat{\epsilon} - \epsilon = -\frac{1}{\pi}\arg[\sum_{n=0}^{L-1} S\{r_{\hat{d}+n} r^*_{\hat{d}+n+L}\}e^{i\pi\epsilon}]. \tag{3.51}$$

As we are interested in the variance of CFO estimation, given that time synchronization was previously carried out, we can consider $\hat{d} = 0$, without loss of generality. Besides, as complex factor $e^{i\pi\epsilon} \in \mathbb{C}_i$, it can be placed inside the simplex operator. Therefore,

$$\hat{\epsilon} - \epsilon = -\frac{1}{\pi} \arctan \left(\frac{\mathcal{I}_m[\sum_{n=0}^{L-1} S\{r_n r_{n+L}^* e^{i\pi\epsilon}\}]}{\mathcal{R}_e[\sum_{n=0}^{L-1} S\{r_n r_{n+L}^* e^{i\pi\epsilon}\}]} \right) \tag{3.52}$$

$$= -\frac{1}{\pi} \arctan \left(\frac{\sum_{n=0}^{L-1} \mathcal{I}_i[r_n r_{n+L}^* e^{i\pi\epsilon}]}{\sum_{n=0}^{L-1} \mathcal{R}[r_n r_{n+L}^* e^{i\pi\epsilon}]} \right), \tag{3.53}$$

which, for SNR high enough to produce small estimation errors, it reduces to

$$\hat{\epsilon} - \epsilon \approx -\frac{1}{\pi} \frac{\sum_{n=0}^{L-1} \mathcal{I}_i[r_n r_{n+L}^* e^{i\pi\epsilon}]}{\sum_{n=0}^{L-1} \mathcal{R}[r_n r_{n+L}^* e^{i\pi\epsilon}]}. \tag{3.54}$$

Besides, by repeating (3.48) for convenience,

$$r_n r_{n+L}^* e^{i\pi\epsilon} = |y_n|^2 + y_n z_{n+L}^* e^{i\pi\epsilon} + z_n y_n^* + z_n z_{n+L}^* e^{i\pi\epsilon}, \tag{3.55}$$

leads up to $E[r_n r_{n+L}^* e^{i\pi\epsilon}] = |y_n|^2$, due to independence between signal and noise, and to the fact of z_n is WGN.

In (3.55), it should be noted that the last term corresponds to a product of two i.i.d. quaternion Gaussian r.v.'s, namely z_n and $z_{n+L}^* e^{i\pi\epsilon}$. At high SNR, the p.d.f. of this term becomes more concentrated around the origin of 4D space than its individual factors, which appear in second and third terms weighted by deterministic signal samples y_n and y_n^*, respectively. In other words, at high SNR, the last term is distributed over a 4D sphere of ratio much lower than for the second and third terms. Thus, for the sake of simplicity, we can henceforth ignore the last term. Also, notice that the first term on the right side of (3.55) is deterministic, since expected values are taken with respect to noise components, so let

$$\alpha_n = y_n z_{n+L}^* e^{i\pi\epsilon} + z_n y_n^*, \tag{3.56}$$

the random part of $r_n r_{n+L}^* e^{i\pi\epsilon}$ in (3.55). Under the assumption that both z_n and z_{n+L} are circularly symmetric and independent, it follows that α_n is also circularly symmetric, i.e. its real and three imaginary parts are zero-mean i.i.d. Gaussian real r.v.'s. Thus, numerator and denominator at right side of (3.54) are independent, so that expected value can be distributed, then it follows that $E[\hat{\epsilon} - \epsilon] \approx 0$, i.e., the estimator is unbiased, and $\mathrm{Var}[\hat{\epsilon}] = E[(\hat{\epsilon} - \epsilon)^2]$ reduces to

$$\mathrm{Var}[\hat{\epsilon}] = \frac{1}{\pi^2} \frac{E\left[\left(\sum_{n=0}^{L-1} \mathcal{I}_i[\alpha_n]\right)^2\right]}{E\left[\left(\sum_{n=0}^{L-1} (|y_n|^2 + \mathcal{R}[\alpha_n])\right)^2\right]}. \tag{3.57}$$

As aforementioned, real and imaginary parts of α_n are zero-mean Gaussian real r.v.'s, each one with variance equal to a quarter of VAR$[\alpha_n]$, i.e.,

$$\textsc{Var}[\mathcal{R}[\alpha_n]] = \textsc{Var}[\mathcal{I}_i[\alpha_n]] = \frac{1}{4}E\Big[|\alpha_n|^2\Big] \tag{3.58}$$

$$= \frac{1}{4}E\Big[|y_n|^2|z_{n+L}|^2 + |z_n|^2|y_n|^2 + y_n z^*_{n+L} e^{i\pi\epsilon} y_n z^*_n + z_n y^*_n e^{-i\pi\epsilon} z_{n+L} y^*_n\Big] \tag{3.59}$$

$$= \frac{1}{4}|y_n|^2\Big(E[|z_{n+L}|^2] + E[|z_n|^2]\Big) = \frac{\sigma^2}{2}|y_n|^2. \tag{3.60}$$

This result, along with the independence between α_n and α_m, for $n \neq m$, implies that

$$\sum_{n=0}^{L-1} \mathcal{I}_i[\alpha_n] \sim N(0, \frac{\sigma^2}{2}\sum_{n=0}^{L-1}|y_n|^2) \tag{3.61}$$

$$\sum_{n=0}^{L-1}(|y_n|^2 + \mathcal{R}[\alpha_n]) \sim N(\sum_{n=0}^{L-1}|y_n|^2, \frac{\sigma^2}{2}\sum_{n=0}^{L-1}|y_n|^2). \tag{3.62}$$

Therefore, (3.57) reduces to

$$\textsc{Var}[\hat{\epsilon}] = \frac{1}{\pi^2}\frac{\frac{\sigma^2}{2}\sum\limits_{n=0}^{L-1}|y_n|^2}{\frac{\sigma^2}{2}\sum\limits_{n=0}^{L-1}|y_n|^2 + \left(\sum\limits_{n=0}^{L-1}|y_n|^2\right)^2} \tag{3.63}$$

$$= \left[\pi^2\left(1 + \frac{\sum\limits_{n=0}^{L-1}|y_n|^2}{\sigma^2/2}\right)\right]^{-1}. \tag{3.64}$$

In the above equation, for L high enough, an approximation of the sum of the numerator is $L\sigma_y^2$, where σ_y^2 is the mean power of the signal. Using this result, (3.64) expressed in terms of SNR $= \sigma_y^2/\sigma^2$ gives

$$\textsc{Var}[\hat{\epsilon}] = \frac{1}{\pi^2(1 + 2L\ \text{SNR})}, \tag{3.65}$$

which, for high SNR, gives the bound

$$\text{CRLB} = \frac{1}{2\pi^2 L\ \text{SNR}}. \tag{3.66}$$

3.3 Conclusions

This chapter presented synchronization techniques for dual-polarized QOFDM systems, based on classical OFDM synchronization algorithms. These techniques were divided into that based on training symbols, inspired in the Schmidl & Cox algorithm [64], and that based on cyclic prefix, taking Van de Beek's work [58] as reference.

In general, the use of quaternions allowed compact and elegant representations for dual-polarized signals. Moreover, quaternion techniques exhibited improved performance for estimation of CFO and STO, both in cyclic prefix and training symbol scenarios; as expected due to diversity gain and the efficient use of quaternion algebra. In the STO estimation, this gain is expressed as a double slope in the logarithmic-scale graph variance vs. SNR, when compared to single polarization and to the independent-double estimates case.

For all scenarios, the CRLB was calculated for STO and CFO estimates, and Monte Carlo simulations were performed in order to validate these results. As expected, the proposed techniques produce unbiased estimators that successfully achieve their corresponding CRLB for high SNR values. For low SNR, the generalized Barankin bound (BB) can be used [66], but for the sake of simplicity, these cases were left out of the scope of the present thesis.

Although the proposed techniques were fully developed by using quaternion notation, their practical implementations can be carried out using complex algebra. The corresponding complex equations were readily deduced and presented at the end of their respective sections.

Finally, the results obtained in this chapter, by reformulating classic synchronization algorithms, encourage us to consider, in future work, other synchronization methods, such as the use of pilots.

4 MIMO-OFDM using dual-polarized antennas and quaternions

MIMO-OFDM is the main air interface technology used in 4G and 5G mobile communications. In this chapter, we present the application of QODs discussed in Chapter 2, for dual-polarized MIMO OFDM systems, in order to implement flexible combinations of space, time, and polarization diversity schemes. Section 4.1 summarizes the basics of MIMO systems using OFDM from a classic perspective; the quaternion MIMO OFDM scheme is presented in Section 4.2. Finally, Section 4.3 exhibits the simulation results for different scenarios of combined diversities.

4.1 MIMO OFDM review

OFDM is a modulation technique widely used in wireless communications. Its implementation uses discrete Fourier transforms (DFTs) to transform a frequency-selective fading channel into several flat fading sub-channels in the frequency domain, thus leading to efficient use of the radio spectrum and, consequently, providing high data rates transmission. OFDM is found in a number of modern communications systems such as wireless mobile communications, broadcasting of digital radio and television signals, and wireless local area network (LAN). The discrete Fourier transform can also be viewed as a modulation technique with several transmit subcarriers, which are equally spaced in frequency; these subcarriers are defined by the base functions of the transform. For transmission, not all subcarriers are used for data modulation: some are reserved as guard frequencies to provide robustness against interference from adjacent channels (N_g), and some are reserved for synchronization of pilot subcarriers (N_p). Pilot carriers are also used for channel equalization. Message bit-streams are grouped for modulating subcarriers of all other Fourier transform base functions (consisting of N_l payload subcarriers).

In the transmitter, serial-to-parallel data conversion allows mapping of the message bit-stream according to the constellation in the modulation, so as to form a discrete Fourier transform vector of size $N = N_l + N_g + N_p$. Generally, N is chosen to be a power of 2 to take the advantage of fast Fourier transform algorithms. Thus, OFDM can be viewed as a block or symbol vector transmission system. For each OFDM symbol, N carriers are prepared for computing the inverse Fourier transform. Therefore, this vector is time-dependent, changing at mT_s for each OFDM symbol period T_s, and containing N subcarriers, that is,

$$\boldsymbol{X}_m = [X_m[0] \quad X_m[1] \quad \dots \quad X_m[N-1]]^{\mathcal{T}}, \tag{4.1}$$

where $\mathcal{T}$ represents the vector transpose. This vector is then submitted to the inverse Fourier transform. In the time domain, the last N_c block samples are repeated at their beginning, creating a cyclic extension which is used as a time guard interval. Typically, N_c is chosen to be 1/4, 1/8, 1/16, or 1/32 of the size N of the FFT. Therefore, in the time domain, the OFDM symbol has a length of $N_s = N + N_c$, which is cyclically extended into a vector

$$\boldsymbol{x}_m^c = [x_m[N - N_c] \dots x_m[N-1]\, x_m[0] \dots x_m[N-1]]^{\mathcal{T}}. \tag{4.2}$$

It is important to note that it is possible to use different modulation techniques for different groups of subcarriers. Note that during the period $T_s = N_s T$, the vector $\boldsymbol{x}_m^c$ is serially transmitted by the sequence $x[n]$, where T is the sampling period.

In typical OFDM modulation, the signal sequence $x[n]$ is transmitted through a frequency-selective fading channel of duration equivalent to LT, such that the causal response of the channel link is $h_m[n] = 0$, for $n < 0$ and for $n > L$. To avoid inter-symbol interference, the time guard interval is $N_c \geq L$. Typically, we assume that the channel response is invariant during the OFDM symbol period, in which case, the receive signal is simply the convolution of $h_m[n]$ with the sequence $x[n]$, i.e., $y[n] = x[n] * h_m[n]$; however, $h_m[n]$ varies for each symbol m. At the receiver side, the sequence $y[n]$ is segmented symbol-to-symbol, resulting in the sequence $y_m^c[n]$.

After removing the cyclic samples of the time guard interval, one obtains a received time vector of size N

$$\boldsymbol{y}_m = [y_m^c[N_c] \quad y_m^c[N_c+1] \quad \dots \quad y_m^c[N_c+N-1]]^{\mathcal{T}}. \tag{4.3}$$

Convolution in the time domain corresponds to the product in the DFT domain, that is, for the cyclic-prefix-removed sequences,

$$Y_m[k] = X_m[k]H_m[k] + Z_m[k], \quad k = 0, 1, \dots, N-1, \tag{4.4}$$

where $H_m[k]$ is the DFT of $h_m[n]$, and $Z_m[k]$ is the DFT of the channel noise at OFDM symbol m. This expression can be expressed in matrix form as

$$\boldsymbol{Y}_m = \mathbf{X}_m \boldsymbol{H}_m + \boldsymbol{Z}_{\boldsymbol{m}}, \tag{4.5}$$

where $\mathbf{X}_m$ is a diagonal matrix whose elements are the DFT sequence $X_m[k]$, $\boldsymbol{H}_{\boldsymbol{m}}$ and $\boldsymbol{Z}_{\boldsymbol{m}}$ are, respectively, the frequency response of the channel and the DFT of the channel noise, both referred to the OFDM symbol m. This equation means that the OFDM with a cyclic prefix transforms a frequency-selective fading channel into N perfectly flat fading sub-channels.

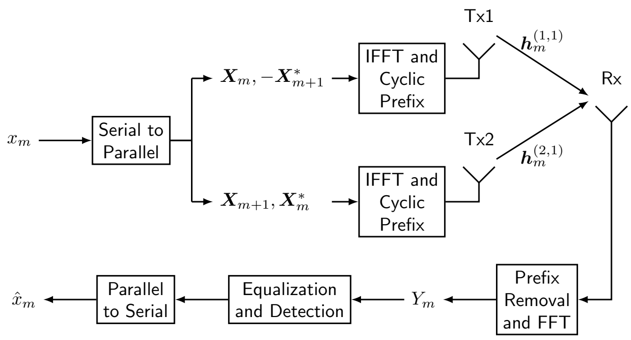

Figure 4.1 – Space-time OFDM transmit diversity system.

4.1.1 Transmit diversity in time domain

MIMO technique has been introduced to classical OFDM. The direct extension of Alamouti space-time coding to this modulation [67] requires two OFDM symbols, as shown in Figure 4.1. This code application achieves diversity gains over frequency-selective fading channels. Note that this scheme will use one OFDM engine for each transmitting antenna. Therefore, after the serial-to-parallel conversion block, two data blocks are created

$$\mathbf{X}_m = \text{diag}\{X_m[0], X_m[1], \ldots, X_m[N-1]\},$$
$$\mathbf{X}_{m+1} = \text{diag}\{X_{m+1}[0], X_{m+1}[1], \ldots, X_{m+1}[N-1]\}.$$

At the upper transmitter in the first OFDM symbol time slot, $\mathbf{X}_m$ is transmitted, followed by $-\mathbf{X}_{m+1}^*$ in the second time slot. At the second transmitter, $\mathbf{X}_{m+1}$ is transmitted first, followed by $\mathbf{X}_m^*$.

The equivalent space-time block code transmit matrix is

$$\mathbf{C} = \begin{bmatrix} \mathbf{X}_m & \mathbf{X}_{m+1} \\ -\mathbf{X}_{m+1}^* & \mathbf{X}_m^* \end{bmatrix},$$

whose elements are the OFDM symbol matrices and their conjugates. The first row of the matrix $\mathbf{C}$ corresponds to time slot m and the second row corresponds to time slot $m+1$; the first column of the matrix $\mathbf{C}$ corresponds to the signal transmitted from the 1$^{\text{st}}$ antenna and the second column from the 2$^{\text{nd}}$ antenna. Because $\boldsymbol{H}_m^{(1,1)}$ and $\boldsymbol{H}_m^{(2,1)}$ are the respective DFTs of the channel unit responses $h_m^{(1,1)}[n]$ and $h_m^{(2,1)}[n]$, where $h_m^{(r,s)}[n]$ represents the channel fading gain of the link from transmit antenna r to receive antenna s, and because these responses are considered constant during two consecutive OFDM symbol periods, the correspondent received vectors is given by $\boldsymbol{Y} = \mathbf{C}\boldsymbol{H} + \boldsymbol{Z}$, or, explicitly,

$$\begin{bmatrix} \boldsymbol{Y}_m \\ \boldsymbol{Y}_{m+1} \end{bmatrix} = \begin{bmatrix} \mathbf{X}_m & \mathbf{X}_{m+1} \\ -\mathbf{X}_{m+1}^* & \mathbf{X}_m^* \end{bmatrix} \begin{bmatrix} \boldsymbol{H}_m^{(1,1)} \\ \boldsymbol{H}_m^{(2,1)} \end{bmatrix} + \begin{bmatrix} \boldsymbol{Z}_m \\ \boldsymbol{Z}_{m+1} \end{bmatrix},$$

where $\boldsymbol{Z_m}$ and $\boldsymbol{Z_{m+1}}$ are noise components. By rearranging the above equation, one can write

$$\begin{bmatrix} \boldsymbol{Y}_m \\ \boldsymbol{Y}_{m+1}^* \end{bmatrix} = \begin{bmatrix} \mathbf{H}_m^{(1,1)} & \mathbf{H}_m^{(2,1)} \\ \mathbf{H}_m^{(2,1)*} & -\mathbf{H}_m^{(1,1)*} \end{bmatrix} \begin{bmatrix} \boldsymbol{X}_m \\ \boldsymbol{X}_{m+1} \end{bmatrix} + \begin{bmatrix} \boldsymbol{Z}_m \\ \boldsymbol{Z}_{m+1}^* \end{bmatrix}, \tag{4.6}$$

where $\mathbf{H}_m^{(1,1)}$ and $\mathbf{H}_m^{(2,1)}$ are diagonal matrices, and $\boldsymbol{X}_m$ and $\boldsymbol{X}_{m+1}$ are column vectors. By neglecting noise components in the above equation, estimates $\hat{\boldsymbol{X}}_m$ and $\hat{\boldsymbol{X}}_{m+1}$ of the transmitted information at receiver are

$$\begin{bmatrix} \hat{\boldsymbol{X}}_m \\ \hat{\boldsymbol{X}}_{m+1} \end{bmatrix} = \mathcal{H}_m \begin{bmatrix} \boldsymbol{Y}_m \\ \boldsymbol{Y}_{m+1}^* \end{bmatrix} = \delta^{-1} \begin{bmatrix} \mathbf{H}_m^{(1,1)*} & \mathbf{H}_m^{(2,1)} \\ \mathbf{H}_m^{(2,1)*} & -\mathbf{H}_m^{(1,1)} \end{bmatrix} \begin{bmatrix} \boldsymbol{Y}_m \\ \boldsymbol{Y}_{m+1}^* \end{bmatrix}, \tag{4.7}$$

where $\mathcal{H}_m$ is the Alamouti linear decoding matrix. This matrix is the inverse of the system matrix in (4.6), and its opposite determinant $\delta = (\|\mathbf{H}_m^{(1,1)}\|_{\mathcal{F}}^2 + \|\mathbf{H}_m^{(2,1)}\|_{\mathcal{F}}^2)$ is the sum of the Frobenius norm of the respective channels. Explicitly, these estimates are, by inserting (4.6) in (4.7), given by

$$\begin{aligned} \hat{\boldsymbol{X}}_m &= \delta^{-1}(\mathbf{H}_m^{(1,1)*}\boldsymbol{Y}_m + \mathbf{H}_m^{(2,1)}\boldsymbol{Y}_{m+1}^*) = \boldsymbol{X}_m + \boldsymbol{Z}_m' \\ \hat{\boldsymbol{X}}_{m+1} &= \delta^{-1}(\mathbf{H}_m^{(2,1)*}\boldsymbol{Y}_m - \mathbf{H}_m^{(1,1)}\boldsymbol{Y}_{m+1}^*) = \boldsymbol{X}_{m+1} + \boldsymbol{Z}_{m+1}', \end{aligned}$$

where $\boldsymbol{Z}_m'$ and $\boldsymbol{Z}_{m+1}'$ are combination of noises filtered by the channel responses. Therefore, these estimates are the transmitted symbols plus noise components filtered by the communication links. The above combined signal-plus-noise components are then sent to the maximum likelihood detector.

4.1.2 Transmitter diversity in the frequency domain

Diversity can also be exploited in the frequency domain [68]. Figure 4.2 presents a block diagram of a system using orthogonal space-frequency block coding with two transmit and one receive antennas. This system is a simple extension of space-time coding to the frequency domain.

As in the case of transmitter diversity in the time domain, one OFDM engine is used for each transmitter antenna. After the serial-to-parallel conversion block, the data symbol $\boldsymbol{X}_m = [X_m[0] \quad X_m[1] \quad \ldots \quad X_m[N-1]]^T$ is Alamouti coded into two matrices as follows

$$\begin{aligned} \mathbf{X}_m^{(1)} &= \mathrm{diag}\{X_m[0], -X_m^*[1], \ldots, X_m[N-2], X_m^*[N-1]\}, \\ \mathbf{X}_m^{(2)} &= \mathrm{diag}\{X_m[1], X_m^*[0], \ldots, X_m[N-1], X_m^*[N-2]\}. \end{aligned}$$

Unlike space-time diversity, in the same OFDM block instant m, $\mathbf{X}_m^{(1)}$ is transmitted from the first antenna while $\mathbf{X}_m^{(2)}$ is transmitted from the second antenna. For a better description of this modulation technique, it is useful to decompose the matrix $\mathbf{X}_m = \mathrm{diag}\{\boldsymbol{X}_m\}$ into its even and odd components using the following notation $\mathbf{X}_m^e$, $\mathbf{X}_m^o$. By doing the same for $\mathbf{X}_m^{(1)}$ and $\mathbf{X}_m^{(2)}$, we obtain $\mathbf{X}_m^{(1)e}$, $\mathbf{X}_m^{(1)o}$, $\mathbf{X}_m^{(2)e}$, and $\mathbf{X}_m^{(2)o}$. Thus, the equivalent space-frequency block coding matrix will be

$$\mathbf{C} = \begin{bmatrix} \mathbf{X}_m^e & \mathbf{X}_m^o \\ -\mathbf{X}_m^{o*} & \mathbf{X}_m^{e*} \end{bmatrix}.$$

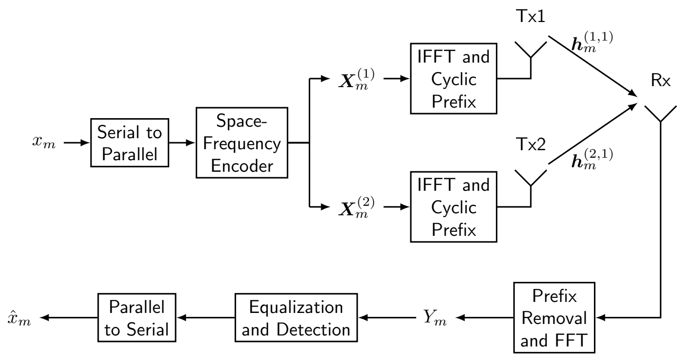

Figure 4.2 – Space-frequency OFDM transmit diversity system.

The received signal vector is $\boldsymbol{Y_m} = \mathbf{C}\boldsymbol{H_m} + \boldsymbol{Z_m}$. In a similar way to that in the previous section, we use a rearranged channel model

$$\boldsymbol{Y}_m = \mathbf{H}_m^{(1,1)}\boldsymbol{X}_m^{(1)} + \mathbf{H}_m^{(2,1)}\boldsymbol{X}_m^{(2)} + \boldsymbol{Z_m},$$

where $\mathbf{H}_m^{(1,1)}$ and $\mathbf{H}_m^{(2,1)}$ are diagonal matrices whose diagonal elements are the respective unit responses of $h_m^{(1,1)}[n]$ and $h_m^{(2,1)}[n]$. Splitting $\boldsymbol{Y_m}$ into its even and odd components, and doing in similar way for matrices $\mathbf{H}_m^{(1,1)}$ and $\mathbf{H}_m^{(2,1)}$, we obtain

$$\begin{aligned}\boldsymbol{Y}_m^e &= \mathbf{H}_m^{(1,1)e}\boldsymbol{X}_m^{(1)e} + \mathbf{H}_m^{(2,1)e}\boldsymbol{X}_m^{(2)e} + \boldsymbol{Z_m^e}\\ \boldsymbol{Y}_m^o &= \mathbf{H}_m^{(1,1)o}\boldsymbol{X}_m^{(1)o} + \mathbf{H}_m^{(2,1)o}\boldsymbol{X}_m^{(2)o} + \boldsymbol{Z_m^o},\end{aligned}$$

where $\boldsymbol{Z_m^e}$ and $\boldsymbol{Z_m^o}$ are noise components. In a similar way to space-time coding, using linear decoding Alamouti matrix and considering even and odd adjacent propagation channel responses as approximately equal, this conducts, respectively, to the estimates of $\hat{\boldsymbol{X}}_m^e$ and $\hat{\boldsymbol{X}}_m^o$ at the receiver:

$$\begin{aligned}\hat{\boldsymbol{X}}_m^e &= \delta^{-1}(\mathbf{H}_m^{(1,1)e*}\boldsymbol{Y}_m^e + \mathbf{H}_m^{(2,1)e}\boldsymbol{Y}_m^{o*}) = \boldsymbol{X}_m^e + \boldsymbol{Z_m^{e'}}\\ \hat{\boldsymbol{X}}_m^o &= \delta^{-1}(\mathbf{H}_m^{(2,1)e*}\boldsymbol{Y}_m^e - \mathbf{H}_m^{(1,1)e}\boldsymbol{Y}_m^{o*}) = \boldsymbol{X}_m^o + \boldsymbol{Z_m^{o'}},\end{aligned}$$

where $\delta = (\|\mathbf{H}_m^{(1,1)e}\|_{\mathcal{F}}^2 + \|\mathbf{H}_m^{(2,1)e}\|_{\mathcal{F}}^2)$, and $\boldsymbol{Z_m^{e'}}$ and $\boldsymbol{Z_m^{o'}}$ are combinations of filtered noises by the channel responses. These terms are the even and odd components of the estimate $\hat{\boldsymbol{X}}_m$, which are sent to the maximum likelihood detector.

Other SF codes proposed in the literature guarantee full-rate and full-diversity transmission in MIMO-OFDM systems [69].

4.2 MIMO-QOFDM scheme

The proposed MIMO-OFDM system is shown in Fig 4.3. The system uses M_t and M_r dual-polarized antennas on the transmitting and receiving sides, respectively. The diversity encoder splits and encodes the input bit stream according to the QOD and the adopted strategy of diversity.

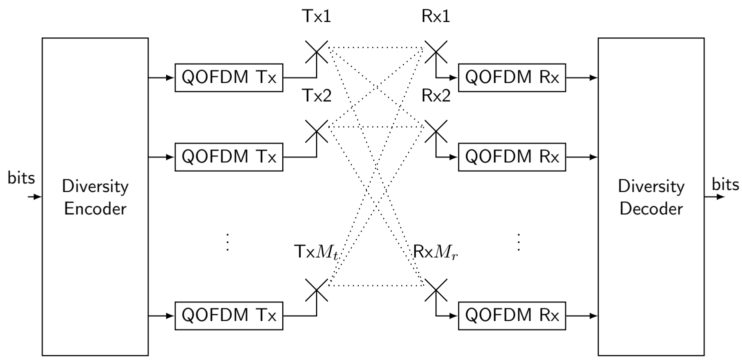

Figure 4.3 – Quaternion MIMO-OFDM system using cross-polarized antennas.

At the transmitter, M_t dual-polarized antennas are used. M_r dual-polarized antennas are used at the receiver. In general, the frequency-selective fading channel for each pair Tx-Rx has L independent delay paths, and this channel remains constant over the QOFDM symbol period. The unit response from the transmit antenna r to the receive antenna s for each pair of elements of the cross-polarized antennas is

$$h_m^{\bowtie(r,s)}[n] = \sum_{l=0}^{L} \alpha_l^{\bowtie(r,s)} \delta(n - n_l^{\bowtie}), \tag{4.8}$$

where $\alpha_l^{\bowtie(r,s)}$ is a complex gain of the l-th path between link r and s, $n_l^{\bowtie}$ is the delay of the l-th path, and symbol $\bowtie$ is a placeholder for hh, hv, vh, or vv polarization cases. The element-to-element channel frequency response is expressed by

$$H_m^{\bowtie(r,s)}[k] = \sum_{l=0}^{L} \alpha_l^{\bowtie(r,s)} e^{-\boldsymbol{j}\frac{2\pi k}{T} n_l^{\bowtie}}, \quad k = 0, 1, ..., N-1, \tag{4.9}$$

where the subcarrier separation is $1/T$, and $\boldsymbol{j}$ is the complex imaginary unit. In this way, a quaternion channel response from transmit antenna r to receive antenna s can be represented by quaternion vector

$$\boldsymbol{H}_m^{\times(r,s)} = [H_m^{\times(r,s)}[0]^{\mathcal{T}} H_m^{\times(r,s)}[1]^{\mathcal{T}} \cdots H_m^{\times(r,s)}[N-1]^{\mathcal{T}}]^{\mathcal{T}}. \tag{4.10}$$

Elements of $\boldsymbol{H}_m^{\times(r,s)}$ can also be separated into vectors for each link of the cross-polarized antennas

$$\boldsymbol{H}_m^{\bowtie(r,s)} = [H_m^{\bowtie(r,s)}[0] H_m^{\bowtie(r,s)}[1] \cdots H_m^{\bowtie(r,s)}[N-1]]^{\mathcal{T}}, \tag{4.11}$$

which are link channel responses in (4.9).

The input bitstreams are pairwise separated into two groups $b_{0,i}$ and $b_{1,i}$, for $0 \leq i \leq N_b$, forming two 2^{N_b}-ary complex symbols, which are mapped onto two perpendicular Argand planes intercepting at the origin of the 4D space [42]. Using the CD composition (2.49), quaternion values $Q_m[k]$, for $k = 0, 1, ..., N-1$ are created. These N quaternions are grouped into a column vector $\boldsymbol{Q}_m$ to be OFDM modulated by using N_l subcarriers.

Table 4.1 – Dimension of several quaternion matrices and vectors for the quaternionic MIMO-OFDM computed based on the number of complex elements

Symbols	Dimensions
$\mathbf{D}$	$M_bNM_r \times 2M_bNM_tM_r$
$\mathcal{D}_i$	$M_bN \times M_bN$
$\boldsymbol{H}$	$M_bNM_tM_r \times 2$
$\boldsymbol{Y}$, $\boldsymbol{Z}$	$M_bNM_r \times 2$

A set of M_b consecutive OFDM blocks, represented by $\boldsymbol{Q}_m$, $\boldsymbol{Q}_{m+1}$, ..., $\boldsymbol{Q}_{m+M_b-1}$, are mapped onto a diversity codeword, which is expressed by the following $M_bN \times M_t$ matrix:

$$\mathbf{C} = \begin{bmatrix} \mathcal{C}_1^{\mathcal{T}} & \mathcal{C}_2^{\mathcal{T}} & \dots & \mathcal{C}_{M_b}^{\mathcal{T}} \end{bmatrix}^{\mathcal{T}}, \tag{4.12}$$

where each element $\mathcal{C}_m$ is defined as

$$\mathcal{C}_m = \begin{bmatrix} C_m^{(1)}[0] & C_m^{(2)}[0] & \dots & C_m^{(M_t)}[0] \\ C_m^{(1)}[1] & C_m^{(2)}[1] & \dots & C_m^{(M_t)}[1] \\ \vdots & \vdots & \ddots & \vdots \\ C_m^{(1)}[N-1] & C_m^{(2)}[N-1] & \dots & C_m^{(M_t)}[N-1] \end{bmatrix}. \tag{4.13}$$

The above $\boldsymbol{Q}_m$ mapping is similar to complex $\boldsymbol{X}_m$ mapping cases in Section 4.1. Each column l of the matrix (4.12) will be transmitted from antenna l after having been processed by an OFDM transmit engine, which applies a quaternionic IFFT (inverse fast Fourier transform) and appends a cyclic prefix. Frequency, time, or both frequency and time diversities are implemented along the rows of $\mathbf{C}$, whereas space and polarization diversities are implemented along the columns of $\mathbf{C}$. From the above matrix codeword, another sparse matrix is defined by

$$\mathbf{D} = \mathbf{I}_{M_r} \otimes [\mathcal{D}_1^s\, \mathcal{D}_1^p\, \mathcal{D}_2^s\, \mathcal{D}_2^p \dots \mathcal{D}_{M_t}^s\, \mathcal{D}_{M_t}^p],$$

where $\otimes$ represents the Kronecker product, $\mathbf{I}_{M_r}$ is the identity matrix of order M_r, and elements $\mathcal{D}_i^s$ and $\mathcal{D}_i^p$ are diagonal matrices defined by

$$\begin{aligned} \mathcal{D}_i^s &= \operatorname{diag}\{\mathcal{S}\{C_m^{(i)}[0]\}, \mathcal{S}\{C_m^{(i)}[1]\}, \dots, \mathcal{S}\{C_m^{(i)}[M_bN-1]\}\}, \\ \mathcal{D}_i^p &= \operatorname{diag}\{\mathcal{P}\{C_m^{(i)}[0]\}, \mathcal{P}\{C_m^{(i)}[1]\}, \dots, \mathcal{P}\{C_m^{(i)}[M_bN-1]\}\}, \end{aligned} \tag{4.14}$$

for $i = 1, 2, ..., M_t$, whose elements are columns of matrix $\mathbf{C}$. Table 4.1 shows the dimension of the above vectors or matrices based on the number of complex elements.

The received signal in matrix form is

$$\boldsymbol{Y} = \sqrt{\frac{\rho}{M_t}}\mathbf{D}\boldsymbol{H} + \boldsymbol{Z}. \tag{4.15}$$

The $\sqrt{\rho/M_t}$ term is used for adjusting the signal-to-noise ratio at a receive antenna to be independent of the number of transmit antennas [69]. The channel $\boldsymbol{H}$ is defined as

$$\boldsymbol{H} = [\boldsymbol{H}^{(1,1)\mathcal{T}} \cdots \boldsymbol{H}^{(M_t,1)\mathcal{T}} \boldsymbol{H}^{(1,2)\mathcal{T}} \cdots \boldsymbol{H}^{(M_t,2)\mathcal{T}} \cdots \boldsymbol{H}^{(1,M_r)\mathcal{T}} \cdots \boldsymbol{H}^{(M_t,M_r)\mathcal{T}}]^{\mathcal{T}}, \quad (4.16)$$

where $\boldsymbol{H}^{(r,s)}$ is defined by

$$\boldsymbol{H}^{(r,s)} = [\boldsymbol{H}_m^{\times(r,s)\mathcal{T}} \boldsymbol{H}_{m+1}^{\times(r,s)\mathcal{T}} \cdots \boldsymbol{H}_{m+M_b-1}^{\times(r,s)\mathcal{T}}]^{\mathcal{T}}, \quad (4.17)$$

where $\boldsymbol{H}_m^{\times(r,s)}$ is defined in (4.10), and m indicates the beginning of a block code.

The received signal is

$$\boldsymbol{Y} = [\mathcal{Y}^{(1)\mathcal{T}} \mathcal{Y}^{(2)\mathcal{T}} \cdots \mathcal{Y}^{(M_r)\mathcal{T}}]^{\mathcal{T}}, \quad (4.18)$$

where each element is

$$\mathcal{Y}^{(i)} = \begin{bmatrix} [\mathcal{S}\{Y_m^{(i)}[0]\}, \mathcal{P}\{Y_m^{(i)}[0]\}] \\ \vdots \\ [\mathcal{S}\{Y_m^{(i)}[N-1]\}, \mathcal{P}\{Y_m^{(i)}[N-1]\}] \\ [\mathcal{S}\{Y_{m+1}^{(i)}[0]\}, \mathcal{P}\{Y_{m+1}^{(i)}[0]\}] \\ \vdots \\ [\mathcal{S}\{Y_{m+M-1}^{(i)}[N-1]\}, \mathcal{P}\{Y_{m+M-1}^{(i)}[N-1]\}] \end{bmatrix}. \quad (4.19)$$

The structure of the quaternion noise vector $\boldsymbol{Z}$ is similar to that given above for $\boldsymbol{Y}$. The simplex and perplex parts of the quaternion noise $\boldsymbol{Z}$ are independent and identically distributed zero-mean 2D Gaussian random variables with the same variance. For the presented formulation, since one of the cross-polarized elements is turned off, the equations are reduced to classical complex schemes [70].

4.2.1 Orthogonal diversity codes

The proposed MIMO-OFDM technique presented in the previous section can take advantage of the diversity in several dimensions, i.e., space, time, frequency, and polarization. The first space-time code in OFDM modulation made use of trellis codes [71]. Unlike space-time block codes (STBCs), trellis codes are able to provide both coding gain and diversity gain, and have better bit error rate performance; however, they are more complex than STBCs, because they rely on a Viterbi decoder at the receiver, whereas STBC uses only linear processing. Studies have shown that STBC, which achieves full diversity in quasi-static flat fading channels, can be used to construct space-frequency codes that achieve the maximum diversity available in frequency selective MIMO fading channels [70].

As shown in Chapter 2, a detailed study of the construction of quaternion orthogonal designs was developed in [15].

The QOD suggested in [15] takes two CODs$(2,2)$ (complex orthogonal design) that are equivalent designs to Alamouti's code [46]

$$\mathbf{A} = \begin{bmatrix} z_1 & z_2 \\ -z_2^* & z_1^* \end{bmatrix} \quad \text{and} \quad \mathbf{B} = \begin{bmatrix} z_2 & z_1 \\ z_1^* & -z_2^* \end{bmatrix},$$

such that applying the Cayley-Dickson construction over the matrices results in

$$\mathbf{C} = \mathbf{A} + \mathbf{B}\boldsymbol{j} = \begin{bmatrix} z_1 + z_2\boldsymbol{j} & z_2 + z_1\boldsymbol{j} \\ -z_2^* + z_1^*\boldsymbol{j} & z_1^* - z_2^*\boldsymbol{j} \end{bmatrix}, \tag{4.20}$$

which is a QOD$(2,2)$ with linear processing on complex variables z_1 and z_2.

In this study, to take advantage of several diversities, it will be of interest to work with orthogonal designs of higher order. One example of QOD(4,4) with linear processing on complex variables z_1, z_2, and z_3 that uses Cayley-Dickson construction is

$$\mathbf{C} = \begin{bmatrix} z_3 - z_1\boldsymbol{j} & -2z_2\boldsymbol{j} & -z_1 + z_3\boldsymbol{j} & -2z_2 \\ 2z_2^*\boldsymbol{j} & z_3 - z_1^*\boldsymbol{j} & 2z_2^* & -z_1^* + z_3\boldsymbol{j} \\ z_1^* + z_3^*\boldsymbol{j} & -2z_2 & z_3^* + z_1^*\boldsymbol{j} & -2z_2\boldsymbol{j} \\ 2z_2^* & z_1 + z_3^*\boldsymbol{j} & 2z_2^*\boldsymbol{j} & z_3^* + z_1\boldsymbol{j} \end{bmatrix}. \tag{4.21}$$

Simplex and perplex parts of quaternion vectors $\boldsymbol{Q}_m, \boldsymbol{Q}_{m+1}, \ldots, \boldsymbol{Q}_{m+M_b-1}$ define complexes z_i in codeword $\mathbf{C}$.

In [15], the QODs obtained over quaternion variables are found to be more general and better suited to achieving full diversity gain for an orthogonal and full rate code. In addition to the CD construction, other methods for designing QODs are *quaternion-commuting variables* and *quaternion amicable designs*. However, for the purposes of this thesis, because of its simplicity, the CD construction technique was applied.

4.2.2 Maximum likelihood decoding

For the most part of the simulations in the next section, maximum likelihood (ML) detection is used. For a given channel (known at the receiver), the ML detector is based on the minimum Euclidean distance between the received signal and all possible transmit symbols. The channel estimation at the receiver is typically implemented by using channel equalizers from special symbols (long prefixes) that are periodically transmitted or from the pilot subcarriers. Thus, the ML detector aims to minimize the norm of $\|\boldsymbol{Y} - \mathbf{C}\boldsymbol{H}\|$.

This process is equivalent to finding a set of symbols $\hat{\mathbf{C}}$ that minimizes the squared norm

$$\begin{aligned}
\|\boldsymbol{Y} - \mathbf{C}\boldsymbol{H}\|^2 &= \mathrm{tr}\{(\boldsymbol{Y} - \mathbf{C}\boldsymbol{H})^{\mathcal{H}}(\boldsymbol{Y} - \mathbf{C}\boldsymbol{H})\} \\
&= \mathrm{tr}\{(\boldsymbol{Y}^{\mathcal{H}} - \boldsymbol{H}^{\mathcal{H}}\mathbf{C}^{\mathcal{H}})(\boldsymbol{Y} - \mathbf{C}\boldsymbol{H})\} \\
&= \mathrm{tr}\{\boldsymbol{Y}^{\mathcal{H}}\boldsymbol{Y} - \boldsymbol{Y}^{\mathcal{H}}\mathbf{C}\boldsymbol{H} - \\
&\quad \boldsymbol{H}^{\mathcal{H}}\mathbf{C}^{\mathcal{H}}\boldsymbol{Y} + \boldsymbol{H}^{\mathcal{H}}\mathbf{C}^{\mathcal{H}}\mathbf{C}\boldsymbol{H}\} \\
&= \mathrm{tr}\{\boldsymbol{Y}^{\mathcal{H}}\boldsymbol{Y}\} - 2Re\{\mathrm{tr}[\boldsymbol{Y}^{\mathcal{H}}\mathbf{C}\boldsymbol{H}]\} + \\
&\quad \lambda\,\mathrm{tr}\{\boldsymbol{H}^{\mathcal{H}}\boldsymbol{H}\}, \\
&= -2Re\{\mathrm{tr}[\boldsymbol{Y}^{\mathcal{H}}\mathbf{C}\boldsymbol{H}]\},
\end{aligned} \tag{4.22}$$

where, to get to the last equation, it was used that $\mathbf{C}^{\mathcal{H}}\mathbf{C} = \lambda\mathbf{I}$, and also that for a circular constellation, $\boldsymbol{Y}^{\mathcal{H}}\boldsymbol{Y}$ is independent of the transmitted codeword.

4.3 Simulation results

Performance analysis of the quaternion MIMO-OFDM systems was carried out, considering several common channel scenarios: flat channel and selective fading (time and frequency selectivity). In the strict sense, time and frequency spreading in a mobile channel are correlated, but it is common practice to independently analyze these effects, following the wide-sense stationary uncorrelated scattering (WSSUS) assumption [72].

This section presents simulations for complex and quaternion OFDM, where for all of them $N_l = 100$ and quadrature phase-shift keying (QPSK) is used per subcarrier modulation. Experiments were conducted using QOD(2,2) in (4.20) and QOD(4,4) in (4.21). The power normalization for the transceiver antennas is the same as those used by Alamouti [46], where there are four radiating elements (two cross-polarized elements) for the QOD(2,2) and eight elements for QOD(4,4) are considered. The presented results are based on average bit error rate (BER) curves as a function of the SNR per bit.

In the first simulation scenario, channel coefficients were assumed to be known at the receiver and are constant in each OFDM block containing M_b symbols. Channel coefficients are generated as random complex Gaussian i.d.d. variables, with zero mean and unit variance. The results are shown in Figure 4.4, where the *berfit* function of MATLAB was used to plot the continuous curves. Results indicate that for this flat fading Rayleigh channel with AWGN, using QPSK modulation, quaternion orthogonal space-time-polarization block coding (QOSTPBC) transmit systems, and for instance at a BER line of 10^{-3}, substantial diversity gains relative to established techniques are obtained, such as confronting the classic Alamouti's STBC scheme. SNR gains are found to be over 7 dB for QOD(2,2), and over 10 dB for QOD(4,4), these gains are due to the exploration of polarization diversity. We observe that the results presented for QOD(2,2), although using MIMO-OFDM, are very similar to those presented in [15].

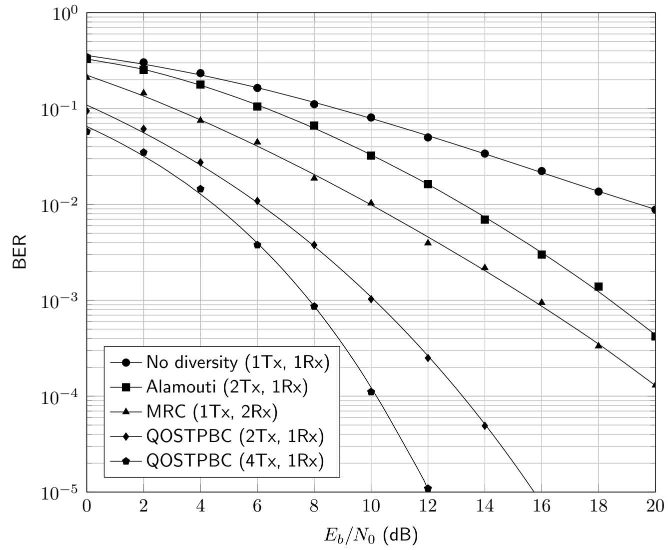

Figure 4.4 – Diversity gain for space-time-polarization transmit systems over a flat fading Rayleigh channel: the first three upper curves consider single elements for Tx and Rx, while QOSTPBC cases consider dual-polarized antennas

Simulation results in Figure 4.5 consider quaternion orthogonal space-time-frequency-polarization block coding (QOSTFPBC) using QOD(4,4) for both mobile and static receivers (i.e., accounting for the Doppler shift or not). Regarding diversity, pairs of columns of $\mathbf{C}$ in (4.21) are grouped for space-frequency-polarization diversity, and pairs of rows of $\mathbf{C}$ are grouped for space-time-polarization diversity. Simulations consider that the unit responses $h_m^{\bowtie(r,s)}[n]$ in (4.8) are independent for hh, hv, vh, and vv links. A maximum Doppler shift of $f_d = 100$ Hz was chosen to represent the relative automobile speeds in an urban environment in the GSM band. For a total bandwidth of 1 MHz, the following four Rayleigh channels were simulated [73]: COST 207, typical urban case with a six-ray profile (TUx6), with and without Doppler shift; and COST 207, typical urban case with twelve-ray profile (TUx12), with and without mobile unit speed. When Doppler shift was considered, it was modeled as a classic Jakes' Doppler spectrum. Channel models in Matlab standard fading functions are used to compute the frame-to-frame unit response for each OFDM symbol. This process yields $\boldsymbol{H}$, which is to be applied to symbol codewords according to (4.15). Although transmission channels are, in theory, assumed to be static over the entire codeword $\mathbf{C}$, vector $\boldsymbol{Y}$ will contain the channel evolution over M_b OFDM symbols and will be degraded by noise components. By contrast, in ML decoding, $\boldsymbol{H}$ is assumed to be static and equal to $\boldsymbol{H}_m$, corresponding to the first OFDM symbol m. This situation simulates the channel equalizer in periods equal to the codeword duration and is updated only at the next codeword. Results for QOSTFPBC transmit systems show very good robustness for these different wireless communication scenarios. In Figure 4.5, we observe that, for a BER line of 10^{-5}, there is a difference between the typical urban case with a six-ray profile using $f_D = 0.001$ Hz and the twelve-ray profile using $f_D = 100$ Hz that is 1.1 dB. Very good discrimination among the four propagation scenarios is observed.

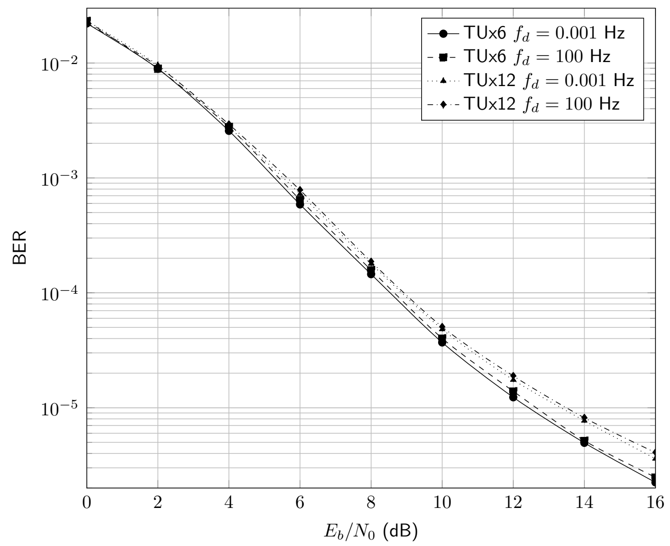

Figure 4.5 – BER for Q(4,4) QOSTFPBC for different wireless communications scenarios.

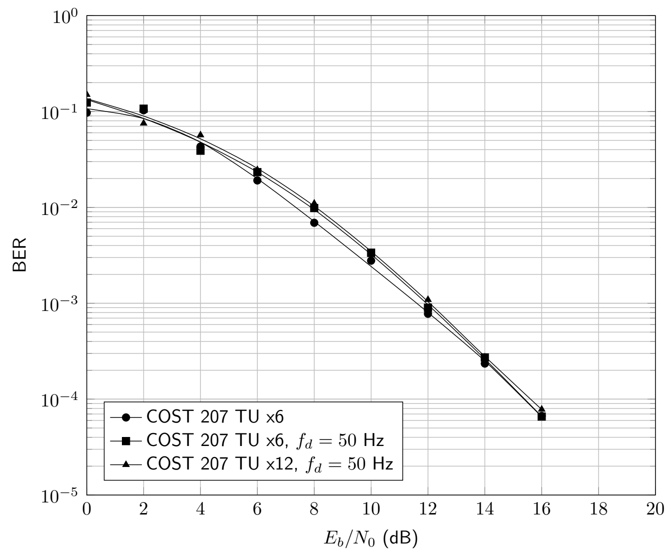

Figure 4.6 – BER for Q(4,4) QOSTFPBC using scattering matrix in different wireless communications scenarios.

When compared with the same QOD(4,4) scheme of Figure 4.4, moderate diversity gains (around 3 dB) are observed for E_b/N_0 up to 8 dB, even not considering the channel state information at the transmitter side (CSIT) or more sophisticated schemes, such as those using beamforming antenna arrays [74].

Simulation results in Figure 4.6 are similar to those of the previous scenario; however, they use matrix (2.52) for different values of parameter cross-polar isolation (XPI) at receive and transmit antennas: $\chi_t = \chi_r = 0$ and χ_r, and $\chi_t = \chi_r = 0.01$, without provision of any mechanism of cross-polar interference cancellation. As long as these cross paths are unknown in the receiver, a degradation in the performance is observed. For example, for a BER level of 10^{-2} dB, the required E_b/N_0 goes, approximately, from 2 dB in Figure 4.5, to 8 dB in Figure 4.6, thus exhibiting a 6 dB performance loss.

Simulations show that QOSTFPBC can efficiently be used for flexible higher spectral efficiency designs, as long as the channel state information is known at receivers (CSIR). As observed in [15], when using well-designed quaternion orthogonal codes, and here by use of quaternion MIMO-OFDM, quaternion schemes are capable of achieving the same performance as complex orthogonal space-time-block codes or complex orthogonal space-frequency-block codes, which would require twice the number of transmitting and receiving antennas.

The last two simulations show that it is possible to consider the communications schemes using independent antenna elements with spatial separation, which represents a doubling in the number of M_t and M_r antennas at transmit and receive sides or using polarized antennas. Therefore, it is possible to group pairs of antennas on both sides to apply the proposed formulation with non-polarized antennas. By contrast, dual-polarized antennas have the advantage of reducing the size of transmitting and receiving antennas.

4.4 Conclusions

This chapter introduced a formulation for MIMO-OFDM using quaternion algebra. The formulation is general and allows us to take advantage of diversities in several domains, such as space, time, frequency, and polarization. The use of orthogonal quaternion code designs of higher order allows us to exploit full diversity in those domains. Several simulations exploring scenarios in typical and severe urban environments, including the Doppler shift in the Jakes spectral model, have been presented. As expected, the use of a higher number of transmit antennas significantly improves the system performance, as could be observed for scenarios using random coefficients for the link frequency responses. Using models for real-world simulations (COST207), satisfactory discrimination of the propagation scenarios can be observed in simulations that are coherent to channel harshness.

It is important to remark that the performance gains of the diversity schemes presented are associated to the different combinations of diversity exploited, and not to the use of quaternions per se. The key role of quaternion in those schemes was to allow the straightforward exploration of until four diversity types, simultaneously, in each scheme.

Finally, the presented formulation applies both to double-polarized antennas and to independent antenna elements that are spatially separated. The presented modulation systems have potential applications in modern wireless communications including next-generation mobile, back-hauling networks, and digital television systems.

5 Concluding remarks

In general, the present research work showed that the use of quaternions to model dual-polarized signals in wireless systems can introduce a number of benefits, including compactness, flexibility, and enhanced performance, among others. On the road to achieving this, we started with a concise review of quaternions presented in Chapter 2. Therein, special attention was put on the discrete QFT as well as on the recently introduced dual-polarized QOFDM scheme. Subsequent chapters presented the main contributions of our research, focusing on two relevant problems related to MIMO and OFDM, which are fundamental components for actual and future communications systems. Namely, synchronization algorithms for dual-polarized systems implementing QOFDM, and flexible diversity schemes for MIMO OFDM systems with dual-polarized antennas, using quaternion OSTPBC's.

From the study of synchronization techniques for QOFDM, some conclusions can be remarked.

> The use of quaternion algebra in synchronization of QOFDM systems allows a simple derivation of joint estimation algorithms that exhibits improved performance when compared to the complex OFDM case. Although different approaches could lead to similar results, it was the quaternion representation of signals and transforms that guided the word towards the presented synchronization algorithms.
>
> Furthermore, in the case of STO estimation using the redundancy provided by the cyclic prefix, the performance gain of the estimator, expressed by a double slope in the log-scale figure variance vs. BER, is far from obvious. A discussion about this result and the corresponding CRLB calculations that support those results were also presented.
>
> Even though, in the present thesis, we took classical synchronization algorithms for OFDM as a reference, similar developments can be carried out for potentially every synchronization technique.

Moreover, the research on QODs applied to MIMO QOFDM allows us to conclude that

> QODs enable a flexible combination of space, time, frequency, and polarization diversities in MIMO dual-polarized systems that can be very useful in mobile environments.

In a scenario with perfect knowledge of channel state information and cross-polar interference cancellation, the Doppler effect produces only small degradation in the overall performance of the proposed diversity schemes. However, when a residual cross-polar interference is considered, the Doppler effect becomes relevant in the intermediate range of E_b/N_0 analyzed.

Finally, throughout the research work, some potential research areas were identified, among them:

i) the use of cyclic prefix-based synchronization techniques to estimate time difference of arrival (TDOA) in mobile scenarios, in order to improve the user equipment localization required by beamforming systems;

ii) the application of quaternion adaptive filters in channel estimation and equalization;

iii) the introduction of quaternion in massive MIMO systems.

Bibliography

1 MELONI, L.; LENZI, K. Performance measurement simulations for analog-to-digital converters. *IEEE Latin America Trans.*, v. 10, n. 1, p. 1168–1174, 2012. Citado 4 vezes nas páginas 16, 18, 19, and 41.

2 MOOSE, P. A technique for orthogonal frequency division multiplexing frequency offset correction. *IEEE Transactions on Communications*, v. 42, n. 10, p. 2908–2914, 1994. Citado 3 vezes nas páginas 16, 36, and 57.

3 HAMILTON, W. R. *Elements of Quaternions*. [S.l.]: Cambridge University Press, 2010. (Cambridge Library Collection - Mathematics). Citado 2 vezes nas páginas 17 and 28.

4 RODRIGUES. Des lois géométriques qui régissent les déplacements d'un système solide dans l'espace, et de la variation des coordonnées provenant de ces déplacements considérés indépendamment des causes qui peuvent les produire. *Journal de Mathématiques Pures et Appliquées*, p. 380–440, 1840. Disponível em: <http://eudml.org/doc/234443>. Citado na página 17.

5 ALTMANN, S. L. Hamilton, rodrigues, and the quaternion scandal. *Mathematics Magazine*, Taylor & Francis, v. 62, n. 5, p. 291–308, 1989. Disponível em: <https://doi.org/10.1080/0025570X.1989.11977459>. Citado na página 17.

6 PUJOL, J. Hamilton, Rodrigues, Gauss, Quaternions, and Rotations: a Historical Reassessment. *Communications in Mathematical Analysis*, Mathematical Research Publishers, v. 13, n. 2, p. 1 – 14, 2012. Disponível em: <https://doi.org/>. Citado na página 17.

7 MAXWELL, J. *A treatise on electricity and magnetism*. New York, NY: Cambridge University Press, 2010, doi: 10.1017/CBO9780511709340. Citado na página 17.

8 ADLER, S. L. Quaternionic quantum field theory. *Communications in Mathematical Physics*, Springer, v. 104, n. 4, p. 611 – 656, 1986. Disponível em: <https://doi.org/>. Citado na página 18.

9 LEO, S. D. Quaternions and special relativity. *Journal of Mathematical Physics*, v. 37, n. 6, p. 2955–2968, 1996. Disponível em: <https://doi.org/10.1063/1.531548>. Citado na página 18.

10 FAMILTON, J. C. *Quaternions: a history of complex noncommutative rotation groups in theoretical physics*. 2015. Citado na página 18.

11 ELL, T. A. *Hypercomplex Spectral Transformations*. Tese (Doutorado) — University of Minnesota, USA, 1992. Citado 2 vezes nas páginas 18 and 29.

12 ELL, T.; SANGWINE, S. Hypercomplex Fourier transform of colour images. *IEEE Trans. Image Process.*, v. 16(1), p. 22–35, January 2007, doi: 10.1109/ICIP.2001.958972. Citado na página 18.

13 SAID, S.; BIHAN, N. L.; SANGWINE, S. Fast complexified quaternion fourier transform. *IEEE Trans. on Signal Processing*, v. 56, n. 4, p. 1522–1531, 2008, doi: 10.1109/TSP.2007.910477. Citado na página 18.

14 WYSOCKI, B. J.; WYSOCKI, T. A.; SEBERRY, J. Modeling dual poralization wireless fading channels using quaternions. *Proc. Symp. on Trends in Communications*, v. 1, n. 1, p. 68–71, 2006, doi: 10.1109/TIC.2006.1708024. Citado 2 vezes nas páginas 18 and 34.

15 SEBERRY, J. et al. The theory of quaternion orthogonal designs. *IEEE Trans. on Signal Processing*, v. 56, p. 256–265, 2008, doi: 10.1109/TSP.2007.906773. Citado 8 vezes nas páginas 18, 36, 38, 39, 68, 69, 70, and 73.

16 GABOR, D. Theory of communication. part 1: The analysis of information. *Journal of the Institution of Electrical Engineers - Part III: Radio and Communication Engineering*, v. 93, p. 429–441(12), November 1946. ISSN 0367-7540. Disponível em: <https://digital-library.theiet.org/content/journals/10.1049/ji-3-2.1946.0074>. Citado na página 18.

17 VILLE, J. Théorie et applications de la notion de signal analytique. *Cables et Transmissions*, p. 61–74, 1948. Citado na página 18.

18 PICINBONO, B. On instantaneous amplitude and phase of signals. *IEEE Transactions on Signal Processing*, v. 45, n. 3, p. 552–560, 1997. Citado na página 18.

19 LE BIHAN, N.; SANGWINE, S. J. *The hyperanalytic signal*. 2010. Citado na página 18.

20 HINOSTROZA, J. L.; MELONI, L. G. P. Envelope recovery in orthocomplex amplitude modulation. In: *2014 14th International Symposium on Communications and Information Technologies (ISCIT)*. [S.l.: s.n.], 2014. p. 318–322. Citado na página 18.

21 MELONI, L.; NINAHUANCA, J. L. H.; JUNIOR, O. T. Construction and analysis of quaternion mimo-ofdm communications systems. *Journal of Communication and Information Systems*, v. 32, n. 1, Sep. 2017. Disponível em: <https://jcis.sbrt.org.br/jcis/article/view/445>. Citado 3 vezes nas páginas 19, 34, and 47.

22 QURESHI, S. S.; ALI, S.; HASSAN, S. A. Linear and decoupled decoders for dual-polarized antenna-based mimo systems. *Sensors*, v. 20, n. 24, 2020. ISSN 1424-8220. Disponível em: <https://www.mdpi.com/1424-8220/20/24/7141>. Citado na página 19.

23 TOOK, C. C.; MANDIC, D. P. The quaternion LMS algorithm for adaptive filtering of hypercomplex processes. *IEEE Transactions on Signal Processing*, v. 57, n. 4, p. 1316–1327, 2009. Citado 2 vezes nas páginas 19 and 31.

24 MANDIC, D. P.; JAHANCHAHI, C.; TOOK, C. C. A quaternion gradient operator and its applications. *IEEE Signal Processing Letters*, v. 18, n. 1, p. 47–50, 2011. Citado 4 vezes nas páginas 19, 26, 31, and 32.

25 LE BIHAN, N.; MARS, J. Singular value decomposition of quaternion matrices: a new tool for vector-sensor signal processing. *Signal Processing*, v. 84, n. 7, p. 1177–1199, 2004. ISSN 0165-1684. Disponível em: <https://www.sciencedirect.com/science/article/pii/S0165168404000647>. Citado na página 19.

26 MIRON, S.; BIHAN, N. L.; MARS, J. Quaternion-music for vector-sensor array processing. *IEEE Transactions on Signal Processing*, v. 54, n. 4, p. 1218–1229, 2006. Citado na página 19.

27 LIU, W. Channel equalization and beamforming for quaternion-valued wireless communication systems. *J. Frankl. Inst.*, v. 354, p. 8721–8733, 2017. Citado na página 19.

28 NINAHUANCA, J. L. H.; TORMENA JR., O.; MELONI, L. G. P. Improved time and frequency synchronization for dual-polarization ofdm systems. *ETRI Journal*, v. 43, n. 6, p. 978–990, 2021. Disponível em: <https://onlinelibrary.wiley.com/doi/abs/10.4218/etrij.2021-0014>. Citado na página 24.

29 SANGWINE, S.; BIHAN, N. L. Quaternion Polar Representation with a Complex Modulus and Complex Argument Inspired by the Cayley-Dickson Form. *Advances in Applied Clifford Algebras*, Springer Verlag, v. 20, n. 1, p. 111–120, 2010. Disponível em: <https://hal.archives-ouvertes.fr/hal-00515650>. Citado na página 28.

30 ELL, T.; BIHAN, N. L.; SANGWINE, S. *Quaternion Fourier Transforms for Signal and Image Processing*. [S.l.: s.n.], 2014. 1-136 p. Citado 2 vezes nas páginas 28 and 41.

31 HAHN, S. L.; SNOPEK, K. M. *Complex and Hypercomplex Analytic Signals : Theory and Applications*. Artech House, 2017. (Artech House Signal Processing Library). ISBN 9781630811327. Disponível em: <http://search.ebscohost.com/login.aspx?direct=true&db=nlebk&AN=1511852&lang=pt-br&site=eds-live&scope=site>. Citado na página 28.

32 PEI, S.-C.; CHANG, J.-H.; DING, J.-J. Commmutative reduced biquaternions and their Fourier transform for signal and image processing applications. *IEEE Trans. on Signal Processing*, v. 52, n. 7, p. 2012–2031, 2004. Citado na página 29.

33 DELSUC, M. A. Spectral representation of 2D NMR spectra by hypercomplex numbers. *Journal of Magnetic Resonance*, v. 77(1), p. 119–124, March 1988, doi: 10.1016/0022-2364(88)90036-4. Citado na página 29.

34 GRIGORYAN, A. M.; AGAIAN, S. S. Commutative quaternion algebra and dsp fundamental properties: Quaternion convolution and fourier transform. *Signal Processing*, Elsevier B.V., v. 196, 7 2022. ISSN 01651684. Citado na página 29.

35 ELL, T. *Hypercomplex Spectral Transformations*. Tese (Doutorado) — University of Minnesota, 1992. Disponível em: <http://search.proquest.com/docview/304027651/abstract>. Citado na página 29.

36 BIHAN, N. L. *The geometry of proper quaternion random variables*. 2016. Citado na página 30.

37 NEESER, F.; MASSEY, J. Proper complex random processes with applications to information theory. *IEEE Transactions on Information Theory*, v. 39, n. 4, p. 1293–1302, 1993. Citado na página 30.

38 OGUNFUNMI, T. Adaptive Filtering Using Complex Data and Quaternions. *Procedia Computer Science*, Elsevier Masson SAS, v. 61, p. 334–340, 2015. ISSN 18770509. Disponível em: <http://dx.doi.org/10.1016/j.procs.2015.09.152>. Citado na página 31.

39 PICINBONO, B.; CHEVALIER, P. Widely linear estimation with complex data. *IEEE Transactions on Signal Processing*, v. 43, n. 8, p. 2030–2033, 1995. Citado na página 31.

40 BRANDWOOD, D. A complex gradient operator and its application in adaptive array theory. *IEE Proceedings H (Microwaves, Optics and Antennas)*, v. 130, p. 11–16(5), February 1983. ISSN 0143-7097. Disponível em: <https://digital-library.theiet.org/content/journals/10.1049/ip-h-1.1983.0004>. Citado na página 32.

41 KREUTZ-DELGADO, K. The complex gradient operator and the cr-calculus. 06 2009. Citado na página 32.

42 MELONI, L. Hypercomplex OFDM schemes for cross-polarized antennas. *2012 International Symposium on Communications and Information Technologies*, v. 1, n. 1, p. 1–6, 2012, doi: 10.1109/ISCIT.2012.6380951. Citado 6 vezes nas páginas 32, 33, 34, 45, 57, and 66.

43 ISAEVA, O. M.; SARYTCHEV, V. A. Quaternion presentations polarization state. In: . [S.l.]: IEEE, 1995. p. 195–196. Citado na página 34.

44 OESTGES, C. et al. Dual-polarized communications: From propagation models to system performance evaluation. *IEEE Trans. on Wireless Communications*, v. 7, p. 4019–4031, 2008, doi: 10.1109/T–WC.2008.070540. Citado na página 35.

45 KELLER, T.; HANZO, L. Adaptive multicarrier modulation: a convenient framework for time-frequency processing in wireless communications. *Proceedings of the IEEE*, v. 88, n. 5, p. 611–640, 2000. Citado na página 36.

46 ALAMOUTI, S. A simple transmit diversity technique for wireless communications. *IEEE J. Sel. Areas Commun.*, v. 16, n. 8, p. 1451–1458, 1998, doi: 10.1109/49.730453. ISSN 07338716. Citado 4 vezes nas páginas 36, 37, 69, and 70.

47 TAROKH, V.; JAFARKHANI, H.; CALDERBANK, A. Space-time block codes from orthogonal designs. *IEEE Transactions on Information Theory*, v. 45, n. 5, p. 1456–1467, 1999. Citado 2 vezes nas páginas 36 and 38.

48 CALDERBANK, A. R. et al. Construction and analysis of a new 4 x 4 orthogonal space-time block code. In: *Information Theory, 2004. ISIT 2004. Proceedings. International Symposium on*. [S.l.: s.n.], 2004, doi: 10.1109/ISIT.2004.1365346. p. 309–309. Citado na página 38.

49 RADON, J. Lineare scharen orthogonaler matrizen. *Abhandlungen aus dem Mathematischen Seminar der Universität Hamburg*, v. 1, n. 1, p. 1–14, 1922. ISSN 1865-8784. Disponível em: <https://doi.org/10.1007/BF02940576>. Citado na página 38.

50 BRENNAN, D. G. Linear diversity combining techniques. *Proceedings of the IRE*, v. 47, n. 6, p. 1075–1102, 1959. Citado na página 38.

51 ALI, S.; QURESHI, S. S.; HASSAN, S. A. Quaternion codes in mimo system of dual-polarized antennas. *Applied Sciences*, v. 11, n. 7, 2021. ISSN 2076-3417. Disponível em: <https://www.mdpi.com/2076-3417/11/7/3131>. Citado na página 39.

52 WALLIS, J. S. Constructions for amicable orthogonal designs. *Bulletin of the Australian Mathematical Society*, Cambridge University Press, v. 12, n. 2, p. 179–182, 1975. Citado na página 39.

53 WOLFE, W. Amicable orthogonal designs-existence. *Canadian Journal of Mathematics*, Canadian Mathematical Society, v. 28, p. 1006–1020, 10 1976. ISSN 0008-414X. Citado na página 39.

54 GANESAN, G.; STOICA, P. Space-time diversity using orthogonal and amicable orthogonal designs. In: *2000 IEEE International Conference on Acoustics, Speech, and Signal Processing. Proceedings (Cat. No.00CH37100)*. [S.l.: s.n.], 2000. v. 5, p. 2561–2564 vol.5. Citado na página 39.

55 MA QUINGHUI LAN, H. I. H. *IEEE International Conference on Communications : proceedings*. [S.l.]: IEEE Xplore, 2008. ISBN 9781424420759. Citado na página 40.

56 KANTOR, I. L.; SOLODOVNIKOV, A. S. *Hypercomplex Numbers: An Elementary Introduction to Algebras*. [S.l.]: Springer, 1989. Citado na página 41.

57 WARD, J. P. *Quaternions and Cayley Numbers Algebra and Applications*. Dordrecht: Springer Netherlands, 1997. Citado na página 41.

58 VAN DE BEEK, J. J.; SANDELL, M.; BORJESSON, P. ML Estimation of Time and Frequency Offset in OFDM Systems. *IEEE Trans. on Signal Process.*, v. 45, n. 7, p. 1800–1805, Jul 1997. Citado 3 vezes nas páginas 42, 50, and 59.

59 VAN DE BEEK, J. J. et al. A time and frequency synchronization scheme for multiuser OFDM. *IEEE Journal on Selected Areas in Communications*, v. 17, n. 11, p. 1900–1914, Nov 1999. ISSN 0733-8716. Citado na página 42.

60 MARTIN, R. K. et al. Algorithms and Bounds for Distributed TDOA-Based Positioning Using OFDM Signals. *IEEE Transactions on Signal Processing*, v. 59, n. 3, p. 1255–1268, Mar 2011. ISSN 1053-587X. Citado na página 48.

61 ATHAUDAGE, C. R. N.; SATHANANTHAN, K. Cramer-Rao Lower Bound on Frequency Offset Estimation Error in OFDM Systems with Timing Error Feedback Compensation. In: *2005 5th International Conference on Information Communications Signal Processing*. [S.l.: s.n.], 2005. p. 1231–1235. Citado 2 vezes nas páginas 48 and 52.

62 KAY, S. M. *Fundamentals of Statistical Signal Processing: Estimation Theory*. Upper Saddle River, NJ, USA: Prentice-Hall, Inc., 1993. ISBN 0-13-345711-7. Citado 2 vezes nas páginas 50 and 51.

63 LYONS, R. *Understanding Digital Signal Processing*. Englewood Cliffs, NJ, USA: Prentice-Hall, Inc., 2010. ISBN 978-0137027415. Citado na página 52.

64 SCHMIDL, T. M.; COX, D. C. Robust frequency and timing synchronization for OFDM. *IEEE Transactions on Communications*, v. 45, n. 12, p. 1613–1621, Dec 1997. ISSN 0090-6778. Citado 4 vezes nas páginas 53, 55, 57, and 59.

65 IEEE Standard for Low-Rate Wireless Networks. *IEEE Std 802.15.4-2015 (Revision of IEEE Std 802.15.4-2011)*, p. 1–709, 2016. Citado na página 54.

66 BARANKIN, E. W. Locally best unbiased estimates. *The Annals of Mathematical Statistics*, Institute of Mathematical Statistics, v. 20, n. 4, p. 477–501, 1949. ISSN 00034851. Disponível em: <http://www.jstor.org/stable/2236306>. Citado na página 60.

67 LEE, K.; WILLIAMS, D. A space-time coded transmitter divesity technique for frequency selective fading channels. *Proc. IEEE Sensor Array and Multichannel Signal Processing Workshop, Cambridge,MA*, v. 1, n. 1, p. 149–152, 2000, doi: 10.1109/SAM.2000.877987. Citado na página 63.

68 LEE, K.; WILLIAMS, D. A space-Frequency Transmitter Diversity Technique for OFDM Systems. *Proc. Global Telecommun. Conference, Globecom, San Francisco, CA*, v. 3, n. 1, p. 1474–1477, 2000, doi: 10.1109/GLOCOM.2000.891885. Citado na página 64.

69 SU, W.; SAFAR, Z.; LIU, K. J. R. Full-Rate Full Diversity Space-Frequency Codes with Optimum Coding Advantage. *IEEE Trans. on Information Theory*, v. 51, n. 1, p. 229–249, 2005, doi: 10.1109/TIT.2004.839496. Citado 2 vezes nas páginas 65 and 68.

70 SU, W. et al. Obtaining Full-Diversity Space-Frequency Codes From Space-Time Codes via Mapping. *IEEE Trans. on Signal Process.*, v. 51, n. 11, p. 2905–16, 2003, doi: 10.1109/TSP.2003.818200. Citado na página 68.

71 AGRAWAL, D. et al. Space-time coded ofdm for high data-rate wireless communication over wideband channels. *Proc. IEEE Vehic. Tech. Conf.*, p. 2232–36. Citado na página 68.

72 BELLO, P. Characterization of Randomly Time-Variant Linear Channels. *IEEE Trans. Commun.*, v. 11, n. 4, p. 360–393, dec 1963, doi: 10.1109/TCOM.1963.1088793. ISSN 0096-2244. Citado na página 70.

73 FAILLI, M.; COST 207 Management Committee. *COST 207: Digital Land Mobile Radio Communications*. [S.l.]: European Comission, 1989. 386 p. ISBN 9282599469. Citado na página 71.

74 CAIRE, G. et al. Multiuser MIMO Achievable Rates With Downlink Training and Channel State Feedback. *IEEE Transactions on Information Theory*, v. 56, n. 6, p. 2845–2866, Jun 2010. ISSN 0018-9448. Citado na página 72.